Three Orbital Model for the iron-based superconductors

Maria Daghofer,* Andrew Nicholson, Adriana Moreo, and Elbio Dagotto
Department of Physics and Astronomy, The University of Tennessee, Knoxville, TN 37996 and Materials Science and Technology Division, Oak Ridge National Laboratory, Oak Ridge, TN 32831
(Dated: January 29, 2010)

The theoretical need to study the properties of the Fe-based high-T_c superconductors using reliable many-body techniques has highlighted the importance of determining what is the minimum number of orbital degrees of freedom that will capture the physics of these materials. While the shape of the Fermi surface (FS) obtained with the local density approximation (LDA) can be reproduced by a two-orbital model, it has been argued that the bands that cross the chemical potential result from the strong hybridization of three of the Fe 3d orbitals. For this reason, a three-orbital Hamiltonian for LaOFeAs obtained with the Slater-Koster formalism by considering the hybridization of the As p orbitals with the Fe d_{xz}, d_{yz}, and d_{xy} orbitals is discussed here. This model reproduces qualitatively the FS shape and orbital composition obtained by LDA calculations for undoped LaOFeAs when four electrons per Fe are considered. Within a mean-field approximation, its magnetic and orbital properties in the undoped case are here described for intermediate values of J/U. Increasing the Coulomb repulsion U at zero temperature, four different regimes are obtained: *(1)* paramagnetic, *(2)* magnetic $(\pi, 0)$ spin order, *(3)* the same $(\pi, 0)$ spin order but now including orbital order, and finally a *(4)* magnetic and orbital ordered insulator. The spin-singlet pairing operators allowed by the lattice and orbital symmetries are also constructed. It is found that for pairs of electrons involving up to diagonal nearest-neighbors sites, the only fully gapped and purely intraband spin-singlet pairing operator is given by $\Delta(\mathbf{k}) = f(\mathbf{k}) \sum_\alpha d_{\mathbf{k},\alpha,\uparrow} d_{-\mathbf{k},\alpha,\downarrow}$ with $f(\mathbf{k}) = 1$ or $\cos k_x \cos k_y$ which would arise only if the electrons in all different orbitals couple with equal strength to the source of pairing.

PACS numbers: 71.10.-w, 71.10.Fd, 74.20.Rp

I. INTRODUCTION

The discovery of high-T_c superconductivity in a family of iron-based compounds[1–8] is offering a new conceptual framework to study the non-standard pairing mechanism that seems to induce these exotic superconducting states.[9] The magnetism present in several of the parent compounds[10–14] and the high critical temperatures are reminiscent of properties observed in the cuprates.[15] But there are also clear differences, since the parent compounds are metallic[10–14] and the Fermi surface (FS) is determined by more than one orbital.[16–20] The multiorbital nature of the problem poses a challenge to the design of minimal models that can be studied with powerful techniques, such as numerical methods. Ab-initio calculations making use of the local density approximation (LDA) indicate that the five 3d orbitals of Fe strongly hybridize to form the bands that are close to the chemical potential.[16–20] However, the FS appears to be determined by bands that have mostly d_{xz} and d_{yz} character, and this observation has been confirmed by polarized angle resolved photoemission spectroscopy (ARPES) experiments.[21] This supports the notion that the minimum number of orbitals to be considered to study the pnictides could be two. In fact, a two-orbital minimal model has been proposed[22,23] and it has been studied with numerical techniques on small clusters,[23,24] as well as with several other approximations.[22,25–30] Both numerical[23,24] and mean-field[25] calculations indicate that the magnetic metallic regime observed experimentally in the undoped compounds[10–14] is stabilized for intermediate values of the Coulomb repulsion U and the numerical calculations suggest that, upon doping in this regime, the most favored pairing operator is interorbital and has symmetry B_{2g}.[23,24]

On the other hand, several authors have claimed that a two-orbital model may miss important features of the real system.[16,18–20,31] It has been argued that a minimal model for the pnictides should contain at least three orbitals for mainly two reasons: *(i)* A relatively small portion of the electron-pocket FS of LaOFeAs is determined by a band of mostly d_{xy} character and *(ii)* the bands that produce the two hole pockets should be degenerate at the center of the Brillouin zone (BZ), which is not the case when only two orbitals are considered. The important question is how much these shortcomings of the model impact the most relevant properties of the pnictides. The aim of this paper is to construct a three-orbital model that addresses these concerns and compare its properties with the two-orbital case. This is important because in other areas of condensed matter physics, such as the manganites, we have learned that a simple single-orbital model is often sufficient to capture qualitatively the phenomenon of colossal magnetoresistance,[32] while clearly a two-orbital model is still necessary to properly describe additional properties such as the magnetic and orbital order observed in these materials.[32] Similarly the minimal two-orbital model for the pnictides appears to reproduce the experimentally observed magnetic order, and it is interesting to investigate to what extent the inclusion of the third orbital xy modifies these results.

While the pnictides exhibit a structural phase tran-

sition at similar or slightly higher temperature as the onset of antiferromagnetic (AF) order, experiments have not yet addressed the issue of orbital order and also have not provided consensus regarding the symmetry of the pairing operator.[33–51] An investigation of the magnetic and orbital orders, as well as pairing symmetries, that are allowed in a three-orbital model compared to those that are possible in the two-orbital case will shed light on the importance of the role that the additional d_{xy} orbital should play in theoretical discussions.

This paper is organized as follows. In Sec. II, the three-orbital model is introduced. Section III contains a mean-field analysis of the magnetic and orbital properties of the undoped system. Section IV is devoted to the classification and analysis of the spin-singlet pairing operators allowed by the orbital and lattice symmetries. A summary and conclusions are presented in Sec. V.

II. THREE ORBITAL MODEL FOR THE PNICTIDES

As explained in the Introduction, it has been suggested that at least three orbitals may be needed to describe the superconducting pnictides because the bands that determine the Fermi surface of LaOFeAs are mostly composed by orbitals d_{xz}, d_{yz}, and d_{xy}.[16,18–20,31,52] The notation xz, yz, and xy will be used for these orbitals, respectively, for better readability. The need to include at least three orbitals in a realistic model was first pointed out in Ref. 31 where a three-orbital model was constructed using the symmetry properties of the Fe-As planes and LDA results. A shortcoming of that proposed model was that it contained an spurious hole-pocket FS around the M point in the extended BZ notation. It was argued[31] that a fourth orbital should be added to remove the extra pocket. However, it will be shown in Sec. II B that this spurious pocket can actually be removed entirely within a three-orbital model formalism, i.e. without adding a fourth orbital.

One important issue that needs to be addressed is the electronic filling to be used in a three-orbital model. Band calculations have determined that the undoped pnictides contain six electrons distributed among the five $3d$ orbitals of each Fe atom. One procedure to determine the filling for a model with a reduced number of orbitals is to start from the crystal field splitting and fill the levels accordingly from the lowest energy up. In the two-orbital model that considers only the xz and yz orbitals, such a consideration would suggest that half-filling is the correct electronic density,[22–24] because the x^2-y^2 and $3z^2-r^2$ orbitals are assumed to be fully occupied with four of the six electrons and the xy orbital is assumed empty, leaving two electrons to populate the xz and yz orbitals. In addition, this filling assignment is the only one that allows to reproduce the LDA calculated FS. Applying the crystal-field splitting rationale to the three-orbital model with xz, yz, and xy orbitals, this argument leads to a filling of one third (i.e. two electrons in three orbitals).[53] However, for such a filling we have not been able to reproduce the LDA shape of the FS. Thus, the filling must be adjusted to approximately reproduce the FS and the orbital occupation numbers obtained with LDA. In fact, band structure calculations suggest that the three-orbital system should be *more* than half-filled and actually have a filling of roughly two thirds (i.e. four electrons in the three orbitals).[9,54] Our analysis shows that a FS with approximately a similar size for the hole and electron pockets can be obtained both at fillings around one and two thirds (i.e. two and four electrons in the three orbitals), but the two almost degenerate hole-pockets around Γ demand a filling larger than half-filling. Thus, the focus of our effort will be on a filling of 2/3, as in Ref. 52. As it will be discussed below, non-half-filled orbitals allow the *orbital* degree of freedom to be active and actually it has been argued that orbital ordering phenomena may play a role in these materials.[53] This orbital order is unlikely in the half-filled case which is the natural filling for the two[22,23] and four[25] orbital models for the pnictides. Once again, note that some authors have considered half-filling in the three-orbital case,[31] but this leads to the "unwanted" hole pocket around M.

A. Real Space

To construct the tight-binding portion of the three-orbital Hamiltonian for the pnictides, the Slater-Koster procedure described in Ref. 24 will be followed. Nearest-neighbor and diagonal next-nearest-neighbor hoppings will be considered for all the orbitals. It is clear that the hopping terms for the xz and yz orbitals are the same as in the previously discussed two-orbital model,

$$\begin{aligned}
H^{xz,yz} = & -t_1 \sum_{\mathbf{i},\sigma} (d^\dagger_{\mathbf{i},xz,\sigma} d_{\mathbf{i}+\hat{y},xz,\sigma} + d^\dagger_{\mathbf{i},yz,\sigma} d_{\mathbf{i}+\hat{x},yz,\sigma} + h.c.) \\
& - t_2 \sum_{\mathbf{i},\sigma} (d^\dagger_{\mathbf{i},xz,\sigma} d_{\mathbf{i}+\hat{x},xz,\sigma} + d^\dagger_{\mathbf{i},yz,\sigma} d_{\mathbf{i}+\hat{y},yz,\sigma} + h.c.) \\
& - t_3 \sum_{\mathbf{i},\hat{\mu},\hat{\nu},\sigma} (d^\dagger_{\mathbf{i},xz,\sigma} d_{\mathbf{i}+\hat{\mu}+\hat{\nu},xz,\sigma} + d^\dagger_{\mathbf{i},yz,\sigma} d_{\mathbf{i}+\hat{\mu}+\hat{\nu},yz,\sigma} + h.c.) \\
& + t_4 \sum_{\mathbf{i},\sigma} (d^\dagger_{\mathbf{i},xz,\sigma} d_{\mathbf{i}+\hat{x}+\hat{y},yz,\sigma} + d^\dagger_{\mathbf{i},yz,\sigma} d_{\mathbf{i}+\hat{x}+\hat{y},xz,\sigma} + h.c.) \\
& - t_4 \sum_{\mathbf{i},\sigma} (d^\dagger_{\mathbf{i},xz,\sigma} d_{\mathbf{i}+\hat{x}-\hat{y},yz,\sigma} + d^\dagger_{\mathbf{i},yz,\sigma} d_{\mathbf{i}+\hat{x}-\hat{y},xz,\sigma} + h.c.) \\
& - \mu \sum_{\mathbf{i}} (n_{\mathbf{i},xz} + n_{\mathbf{i},yz}),
\end{aligned} \tag{1}$$

while the intra-orbital hoppings for the xy orbital are given by

$$\begin{aligned} H^{xy} = & t_5 \sum_{\mathbf{i},\hat{\mu},\sigma} (d^\dagger_{\mathbf{i},xy,\sigma} d_{\mathbf{i}+\hat{\mu},xy,\sigma} + h.c.) \\ & - t_6 \sum_{\mathbf{i},\hat{\mu},\hat{\nu},\sigma} (d^\dagger_{\mathbf{i},xy,\sigma} d_{\mathbf{i}+\hat{\mu}+\hat{\nu},xy,\sigma} + h.c.) \\ & + \Delta_{xy} \sum_{\mathbf{i}} n_{\mathbf{i},xy} - \mu \sum_{\mathbf{i}} n_{\mathbf{i},xy}, \end{aligned} \tag{2}$$

where Δ_{xy} is the energy difference between the xy and the degenerate xz/yz orbitals. The hybridization between the xz/yz and the xy orbitals is given by

$$\begin{aligned} H^{xz,yz;xy} = & - t_7 \sum_{\mathbf{i},\sigma} [(-1)^{|i|} d^\dagger_{\mathbf{i},xz,\sigma} d_{\mathbf{i}+\hat{x},xy,\sigma} + h.c.] \\ & - t_7 \sum_{\mathbf{i},\sigma} [(-1)^{|i|} d^\dagger_{\mathbf{i},xy,\sigma} d_{\mathbf{i}+\hat{x},xz,\sigma} + h.c.] \\ & - t_7 \sum_{\mathbf{i},\sigma} [(-1)^{|i|} d^\dagger_{\mathbf{i},yz,\sigma} d_{\mathbf{i}+\hat{y},xy,\sigma} + h.c.] \\ & - t_7 \sum_{\mathbf{i},\sigma} [(-1)^{|i|} d^\dagger_{\mathbf{i},xy,\sigma} d_{\mathbf{i}+\hat{y},yz,\sigma} + h.c.] \\ & - t_8 \sum_{\mathbf{i},\sigma} [(-1)^{|i|} d^\dagger_{\mathbf{i},xz,\sigma} d_{\mathbf{i}+\hat{x}+\hat{y},xy,\sigma} + h.c.] \\ & + t_8 \sum_{\mathbf{i},\sigma} [(-1)^{|i|} d^\dagger_{\mathbf{i},xy,\sigma} d_{\mathbf{i}+\hat{x}+\hat{y},xz,\sigma} + h.c.] \\ & - t_8 \sum_{\mathbf{i},\sigma} [(-1)^{|i|} d^\dagger_{\mathbf{i},xz,\sigma} d_{\mathbf{i}+\hat{x}-\hat{y},xy,\sigma} + h.c.] \\ & + t_8 \sum_{\mathbf{i},\sigma} [(-1)^{|i|} d^\dagger_{\mathbf{i},xy,\sigma} d_{\mathbf{i}+\hat{x}-\hat{y},xz,y\sigma} + h.c.] \\ & - t_8 \sum_{\mathbf{i},\sigma} [(-1)^{|i|} d^\dagger_{\mathbf{i},yz,\sigma} d_{\mathbf{i}+\hat{x}+\hat{y},xy,\sigma} + h.c.] \\ & + t_8 \sum_{\mathbf{i},\sigma} [(-1)^{|i|} d^\dagger_{\mathbf{i},xy,\sigma} d_{\mathbf{i}+\hat{x}+\hat{y},yz,\sigma} + h.c.] \\ & + t_8 \sum_{\mathbf{i},\sigma} [(-1)^{|i|} d^\dagger_{\mathbf{i},yz,\sigma} d_{\mathbf{i}+\hat{x}-\hat{y},xy,\sigma} + h.c.] \\ & - t_8 \sum_{\mathbf{i},\sigma} [(-1)^{|i|} d^\dagger_{\mathbf{i},xy,\sigma} d_{\mathbf{i}+\hat{x}-\hat{y},yz,\sigma} + h.c.]. \end{aligned} \tag{3}$$

The hopping parameters t_i in Eqs.(1-3) will be determined by fitting the band dispersion to band structure calculation results. The chemical potential μ is set to a two-thirds filling, as already discussed. The operator $d^\dagger_{\mathbf{i},\alpha,\sigma}$ ($d_{\mathbf{i},\alpha,\sigma}$) creates (annihilates) an electron at site $\mathbf{i}$, orbital $\alpha = xz, yz, xy$, and with spin projection σ. $n_{\mathbf{i},\alpha} = n_{\mathbf{i},\alpha,\uparrow} + n_{\mathbf{i},\alpha,\downarrow}$ are the corresponding density operators. Previously proposed three-orbital models[31,52] only contained the nearest-neighbor (NN) hybridization t_7, but since next-nearest neighbor (NNN) terms are included for the intra-orbital component, as well as for the hybridization between xz and yz, they should also be included in the hybridization with xy. In Sec. II B, it is shown that these NNN terms with hopping t_8 turn out to be *crucial* to provide the proper orbital character for the electron pockets when compared with LDA results. Finally note that the hybridization Eq. (3) contains factors $(-1)^{|i|}$ that arise from the two-iron unit cell of the original FeAs planes.

TABLE I: Parameters for the tight-binding portion of the three-orbital model Eqs.(5) to (10). The overall energy unit is electron volts.

t_1	t_2	t_3	t_4	t_5	t_6	t_7	t_8	Δ_{xy}
0.02	0.06	0.03	−0.01	0.2	0.3	−0.2	$-t_7/2$	0.4

B. Momentum Space

The Hamiltonian Eqs. (1-3) can be transformed to momentum space using $d^\dagger_{\mathbf{k},\alpha,\sigma} = \frac{1}{\sqrt{N}} \sum_{\mathbf{i}} e^{-i\mathbf{k}.\mathbf{i}} d^\dagger_{\mathbf{i},\alpha,\sigma}$, where $\mathbf{k}$ is the wavevector and N the number of sites. Note that the Fourier transformed Hamiltonian is defined in the extended or unfolded BZ.[55,56] As pointed out in Ref. 31, the real-space Hamiltonian presented in Eqs. (1-3) is invariant under a translation along the x or y directions followed by a reflexion about the x-z plane. When the eigenstates of the Hamiltonian are labeled in terms of the eigenvalues of these symmetry operations, then the momentum-space Hamiltonian can be expressed in terms of a pseudocrystal momentum that will be called $\mathbf{k}$ that expands the unfolded BZ that corresponds to a single Fe unit-cell in real space. Note that folding the three bands used here into the reduced diamond-like cell defined in the first quadrant by $k_x + k_y \leq \pi$, and symmetric points in the other three quadrants, doubles the number of bands to six as expected.

Equations (1-3) become in momentum space

$$H_{\rm TB}(\mathbf{k}) = \sum_{\mathbf{k},\sigma,\mu,\nu} T^{\mu,\nu}(\mathbf{k}) d^\dagger_{\mathbf{k},\mu,\sigma} d_{\mathbf{k},\nu,\sigma}, \tag{4}$$

with

$$T^{11} = 2t_2 \cos k_x + 2t_1 \cos k_y + 4t_3 \cos k_x \cos k_y - \mu \tag{5}$$

$$T^{22} = 2t_1 \cos k_x + 2t_2 \cos k_y + 4t_3 \cos k_x \cos k_y - \mu \tag{6}$$

$$\begin{aligned} T^{33} = & 2t_5(\cos k_x + \cos k_y) \\ & + 4t_6 \cos k_x \cos k_y - \mu + \Delta_{xy}, \end{aligned} \tag{7}$$

$$T^{12} = T^{21} = 4t_4 \sin k_x \sin k_y, \tag{8}$$

$$T^{13} = \bar{T}^{31} = 2it_7 \sin k_x + 4it_8 \sin k_x \cos k_y, \tag{9}$$

$$T^{23} = \bar{T}^{32} 2it_7 \sin k_y + 4it_8 \sin k_y \cos k_x \ , \tag{10}$$

where a bar on top of a matrix element denotes the complex conjugate. Since the Hamiltonian for a one-iron unit cell has been considered, then $\mathbf{k}$ runs within the corresponding extended BZ $-\pi < k_x, k_y \leq \pi$.

The hopping parameters t_i and Δ_{xy} were chosen to reproduce the shape of the LaOFeAs FS obtained using

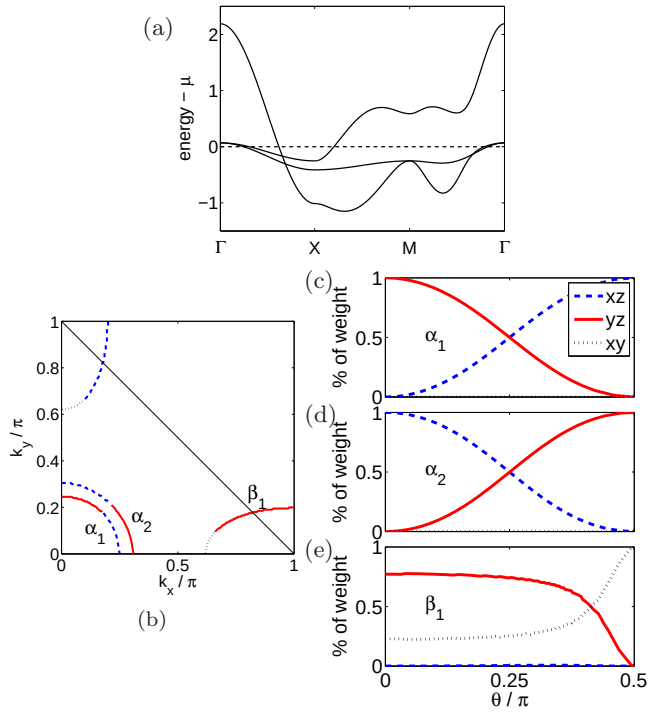

FIG. 1: (Color online) (a) Band structure and (b) Fermi surface of the tight-binding (i.e. non-interacting) three-orbital model, with parameters from Tab. I and in the unfolded BZ. The diagonal thin solid line in (b) indicates the boundary of the folded BZ. In panels (c-e), the orbital contributions to the two hole and one of the electron pockets are given. The winding angle θ is measured with respect to the k_y-axis. The second electron pocket is analogous to the one shown simply replacing xz by yz. In all panels, the dashed lines refer to the xz orbital, the solid to yz, and the dotted to xy.

LDA calculations. These parameters are given in Tab. I. The chemical potential $\mu = 0.212$ was fixed to this value to ensure a filling of two thirds, as discussed in Sec. II. The resulting band dispersion is presented in Fig. 1(a) along high symmetry directions in the extended BZ and the corresponding FS is shown in Fig. 1(b). The two hole-pocket FSs, labeled α_1 and α_2, are formed by two bands that are degenerate at Γ in agreement with LDA, and both of them are found around the Γ-point instead of M in the extended zone. Thus, one of the shortcomings of the two-orbital model has been corrected. It can also be observed that there is no hole-pocket FS around M which was a problem encountered in Refs. 31,52.

The orbital composition of the hole pockets is displayed in Figs. 1 (c) and (d). They are given by a linear combination of the xz and yz orbitals, in agreement with LDA[9,56] and ARPES results.[21] The electron pockets at X (Y) arise from a linear combination of the yz (xz) and xy orbitals. The orbital composition for the electron pocket around X, labeled β_1 in Fig. 1(b), is displayed in Fig. 1(e): here it can be observed that the orbital character changes from purely xy along Γ-X to predominantly yz along X-M, as predicted by LDA[9,56] and also found with ARPES techniques.[21] As can be deduced from Eqs. (9) and (10), setting $t_8 = -t_7/2$ ensures that the electron pockets have pure xy character along the Γ-X and Γ-Y directions.[57] A large yz (xz) contribution along X-M (Y-M) requires the hybridizations t_7 and t_8 to be quite robust.[58]

In summary, a tight-binding Hamiltonian has been constructed that captures the generic shape and orbital composition of the FS for undoped LaOFeAs by considering only the three xz, yz, and xy orbitals, and assuming that they share four of the six electrons that populate the five Fe $3d$ levels.

The Coulombic interacting portion of the Hamiltonian is given by:

$$\begin{aligned} H_{\rm int} = & U \sum_{\mathbf{i},\alpha} n_{\mathbf{i},\alpha,\uparrow} n_{\mathbf{i},\alpha,\downarrow} + (U' - J/2) \sum_{\mathbf{i},\alpha<\beta} n_{\mathbf{i},\alpha} n_{\mathbf{i},\beta} \\ & - 2J \sum_{\mathbf{i},\alpha<\beta} \mathbf{S}_{\mathbf{i},\alpha} \cdot \mathbf{S}_{\mathbf{i},\beta} \\ & + J \sum_{\mathbf{i},\alpha<\beta} (d^\dagger_{\mathbf{i},\alpha,\uparrow} d^\dagger_{\mathbf{i},\alpha,\downarrow} d_{\mathbf{i},\beta,\downarrow} d_{\mathbf{i},\beta,\uparrow} + h.c.), \end{aligned} \tag{11}$$

where $\alpha, \beta = xz, yz, xy$ denote the orbital, $\mathbf{S}_{\mathbf{i},\alpha}$ ($n_{\mathbf{i},\alpha}$) is the spin (electronic density) in orbital α at site $\mathbf{i}$, and the relation $U' = U - 2J$ between these Kanamori parameters has been used (for a discussion in the manganite context see Ref. 32 and references therein). The first line terms give the energy cost of two electrons located in the same orbital or in different orbitals on the same site, respectively. The second line contains the Hund's rule coupling that favors the ferromagnetic (FM) alignment of the spins in different orbitals at the same lattice site. The "pair-hopping" term is in the third line and its coupling is equal to J by symmetry. The values used for U and J can be substantially smaller than the atomic ones, because the interactions may be screened by bands not included in our Hamiltonian. These Coulombic interaction terms have been used and discussed in several previous publications[23–25] where more details can be found by the readers. All the energies in this paper are given in electron volts.

III. NUMERICAL RESULTS

A. Mean-field Approximation and Ordered Phases

To investigate the magnetic and orbital order properties of the three-orbital model in the presence of the onsite Coulomb repulsion, here a mean-field approximation will be used. As it was carried out for the two- and four-orbital models in Ref. 25, here only the mean-field values for diagonal operators will be considered[59] (for details see App. A). In the present case, the degenerate xz and yz orbitals make up most of the weight close to the

TABLE II: Magnetic and orbital ordering wavevectors for the possible ordered phases discussed in the text. The third column indicates the panel of Figs. 2 and 3, where a schematic sketch for the corresponding ordered phase can be found.

spin: q_1	orbital: q_2	panel in Figs. 2 or 3
$(\pi,0)$	$(0,0)$	2(a), 2(b)
(π,π)	$(0,0)$	2(c)
$(\pi,0)$	$(\pi,0)$	2(d), 2(e)
(π,π)	(π,π)	2(f)
$(\pi,0)$	$(0,\pi)$	2(g)
$(\pi,0)$	(π,π)	2(h)
(π,π)	$(\pi,0)$	2(i)
$(0,0)$	$(0,0)$	3(a)
$(0,0)$	$(\pi,0)$	3(b)
$(0,0)$	(π,π)	3(c)

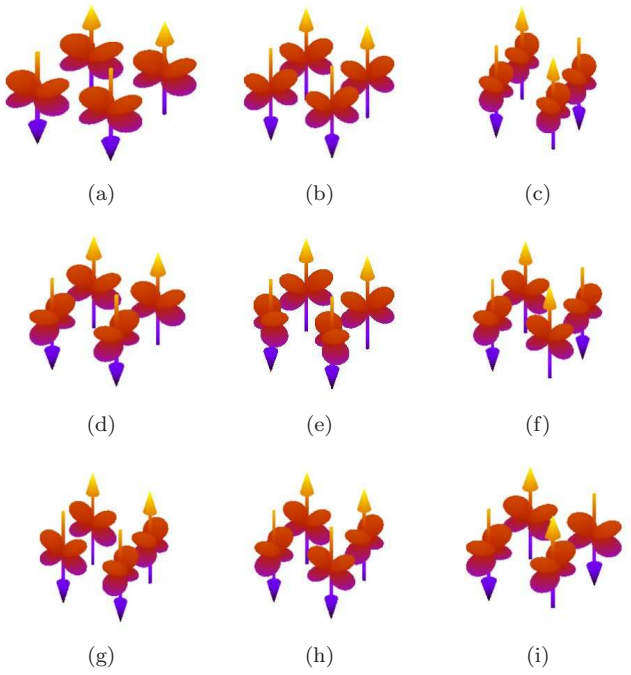

FIG. 2: (Color online) Cartoons representing the spin- and orbital-order configurations considered in this effort. Since four electrons occupy three orbitals, perfectly ordered states have one doubly occupied orbital and the unpaired electrons are located in the other two orbitals, each singly occupied, forming a net spin $S = 1$. In this cartoon, the orbital drawn indicates the doubly occupied one and the arrows indicate the orientation of the total spin at that site. (a) $(\pi, 0)$-spin and ferro-orbital (FO) order favoring the yz orbital, (b) $(\pi, 0)$-spin and FO order favoring $(xz + yz)/\sqrt{2}$, (c) (π, π)-spin and FO order. (d)-(f): states with the same ordering vector for the spins and the orbitals: $(\pi, 0)$ for (d) and (e), (π, π) in (f). (g) $(\pi, 0)$ for spins and $(0, \pi)$ for orbitals; (h) $(\pi, 0)$ for spins and (π, π) for orbitals; (i) (π, π) for spins and $(\pi, 0)$ for orbitals; (b) and (e) illustrate phases where the orbital order does not feature alternating xz and yz orbitals, but the combinations $(xz + yz)/\sqrt{2}$ and $(xz - yz)/\sqrt{2}$ do.

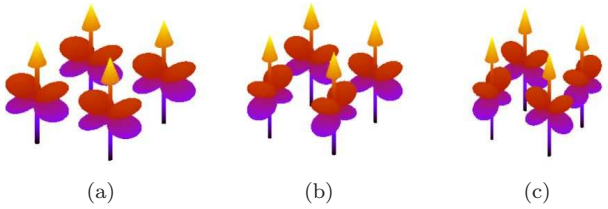

FIG. 3: Color online) Cartoons for the spin ferromagnetic phases taken into consideration in this effort. Results are depicted with the convention of Fig. 2, but for ferromagnetic spins combined with (a) FO, (b) $(\pi, 0)$, and (c) (π, π) orbital order.

chemical potential. In previous investigations of the two-orbital xz-yz model, very weak orbital order has been found within a mean-field approximation at intermediate Coulomb repulsion in the half-filled case, and none in the large-U limit.[29] Numerical simulations did not provide indications of orbital order at half-filling either.[23] However, the xz and yz orbitals are not expected to be half filled in the present case: In the noninteracting $U = 0$ limit, the xy orbital is approximately half filled, so that the subsystem consisting of the two degenerate xz and yz orbitals turns out to be approximately 3/4 filled. Consequently, orbital order within the xz/yz-subspace could now occur, analogously to the case of quarter filling in the xz/yz subsystem.[53]

Three possible orbital-order patterns will be considered: *(i)* Ferro-orbital (FO) order which corresponds to the orbitals xz and yz having different electronic densities, *(ii)* alternating orbital (AO) order, and *(iii)* stripe orbital (SO) order. Combined with the magnetic spin order, these orbital orders lead to a large variety of possible combinations of polarized or alternating spin and orbital order.[60] Here, phases that can be expressed using (at most) two ordering vectors have been considered, i.e. $\mathbf{q}_1$ for magnetic order and $\mathbf{q}_2$ for orbital order. The expectation values for the mean-field proposed states can then be expressed as

$$\langle n_{\mathbf{r},xy,\sigma}\rangle = n_{xy} + \frac{\sigma}{2} e^{i\mathbf{q}_1\cdot\mathbf{r}} m_{xy} \tag{12}$$

$$\langle n_{\mathbf{r},\alpha,\sigma}\rangle = n + \frac{\sigma}{2} e^{i\mathbf{q}_1\cdot\mathbf{r}} m + \frac{\alpha}{2} e^{i\mathbf{q}_2\cdot\mathbf{r}} p + \frac{\sigma\alpha}{2} e^{i(\mathbf{q}_1+\mathbf{q}_2\cdot)\mathbf{r}} q \ , \tag{13}$$

where the first equation with the mean-field parameters n_{xy}, m_{xy} describes the xy orbital and the second equation with parameters n, m, p, and q applies to the xz/yz subsystem, with $\alpha = \pm 1$ indicating the xz/yz orbitals.

The fact that the xz/yz space is not $SU(2)$ symmetric introduces another degree of freedom in addition to the ordering vector: Ferro-orbital order (i.e., site-independent orbital densities) can favor either the xz or yz orbitals [as shown in Fig. 2(a)], or any linear combination $|\phi\rangle = \cos\phi|xz\rangle + \sin\phi|yz\rangle$. As an example, Fig. 2(b) illustrates a state with $\phi = \pi/4$ corresponding to a symmetric combination $(|xz\rangle + |yz\rangle)/\sqrt{2}$. The same holds for

alternating orbital order: alternating order corresponding to $\phi = \pi/4$ can be seen in Fig. 2(e). Consequently, mean-field calculations were performed for several values of ϕ for each phase. The xy orbital might be similarly involved in such a linear combination, because the crystal-field splitting separating it from the xz and yz orbitals is not very large. However, Exact Diagonalization of 2×2 clusters did not give any indication for such behavior: the dominant states in the low-energy eigenstates that we analyzed involved almost exclusively singly occupied or unoccupied xy orbitals. Moreover, the xy orbital is almost singly occupied at $U = 0$ and has low weight at the Fermi energy, so that ordering phenomena in the most relevant intermediate-U regime may be expected to involve mostly xz and yz orbitals. The states considered are shown in Figs. 2 and 3 and the corresponding values of $\mathbf{q}_i$ are given in Tab. II. Which spin-orbital pattern is stabilized depends on the interaction parameters U and J, as described in Sec. III B. The phase with the largest stability range, and which is stable for the most realistic parameter choices, is the $(\pi, 0)$-AF orbital disordered (OD) phase, which will be discussed in more detail in Sec. III C.

B. Magnetic and Orbital Orders in the Undoped Regime

Magnetic order with wavevector $\mathbf{q}_1 = (\pi, 0)$ (or $(0, \pi)$) and OD was found to be stable in a broad - and especially the most realistic - range of interaction parameters. However, the phase diagram in the J/U vs. U plane turns out to contain a large variety of metallic disordered phases, metallic phases with different kinds of magnetic and/or orbital order, and insulating magnetically and orbitally ordered regions. Figure 4 shows a qualitative rendition of the resulting phase diagram. A more accurate quantitative determination of the boundaries as well as a detailed description of all phases will be presented in a future publication. For a realistic Hund's rule coupling $J = U/4$, we discuss the properties of the ground state in the different regimes encountered varying U in Sec. III C below.

It has been found that at large interaction strengths U, after the magnetic order with $\mathbf{q}_1 = (\pi, 0)$ is established, alternating- [$\mathbf{q}_2 = (\pi, \pi)$] and ferro-orbital [$\mathbf{q}_2 = (0, 0)$] order develops for $1/5 \leq J/U \leq 1/3$. For very small values of J/U, ferromagnetic order becomes stable instead of $(\pi, 0)$-antiferromagnetism, and the strongest competitor in the limit $J \to 0$ is $\mathbf{q}_1 = (\pi, \pi)$ antiferromagnetism. At $J = 0$ and for small $3/4 \lesssim U \lesssim 1.5$, both the FM and the (π, π)-AF state have pronounced orbital order corresponding to $\phi = \pi/4$: One of the orbitals given by the linear combinations $(|xz\rangle \pm |yz\rangle)/\sqrt{2}$ is almost filled, the other contains ≈ 1.5 electrons, and xy the remaining 0.5. In the the FM state, $(|xz\rangle + |yz\rangle)/\sqrt{2}$ is the almost filled orbital, while $(|xz\rangle - |yz\rangle)/\sqrt{2}$ has higher occupancy in the (π, π)-AF state with only slightly higher energy. At larger $U > 1.5$, both xz and yz are almost filled for

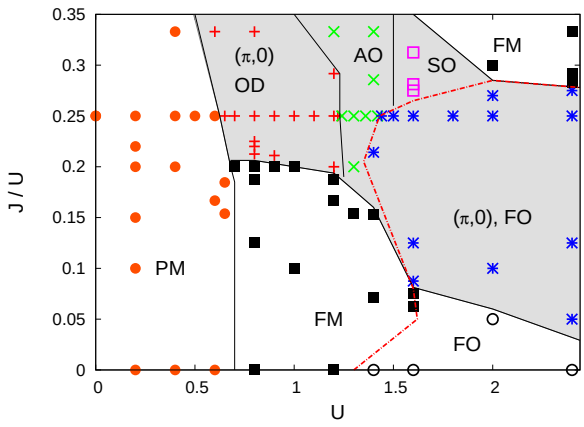

FIG. 4: (Color online) Qualitative phase diagram in the J/U vs. U plane. The shaded area denotes the stability region of the realistic $(\pi, 0)$ magnetic ordering. The lines are guides to the eye, the dashed line approximately indicates the metal-insulator transition. The data points were obtained by comparing the energies of the various phases within the mean-field approximation described in App. A. The meaning of the symbols is the following: +: $(\pi, 0)$-AF state without pronounced orbital order (orbital disorder, OD); ×: $(\pi, 0)$-AF state with (π, π) alternating orbital (AO) order with $\phi = 0$; empty squares: $(\pi, 0)$-AF state with $(0, \pi)$ orbital stripes (SO) ($\phi = 0$); ∗: $(\pi, 0)$-AF state with ferro-orbital (FO) order ($\phi = 0$); filled squares: FM with FO ordering tendencies, $\phi = \pi/4$. This FO order is weaker for small U and larger $J \approx 0.2$. The filled circles denote parameters that do not support magnetically ordered states. For small J, some FO order with $\phi = \pi/4$ is found, similar to the FM phase. The empty circles at large U and small J denote similar states without magnetic ordering, but with extreme orbital order, where the xy orbital is (almost) empty, while xz and yz are (almost) filled.

$J \to 0$, xy is nearly empty, and there are hardly any unpaired spins that could support magnetically ordered phases. Notice that such small ratios of J/U are not expected to be realistic for the pnictides, where the onsite Coulomb repulsion U is strongly screened.[61] With growing J/U, the magnetic ordering vector switches to $(\pi, 0)$ at $J/U \approx 1/5$ for small U, and even smaller J/U for larger U.

For $U \lesssim 2$, the $(\pi, 0)$ magnetic order remains stable for all values of $J/U \gtrsim 1/5$ up to $J/U = 1/3$. At this ratio, the Hund's coupling is such that the inter-orbital repulsion felt by two electrons in different orbitals, but on the same site, vanishes, and we therefore did not consider $J/U > 1/3$.

C. Evolution of the ground state as a function of U for $J = U/4$

In this section, the ground state properties at a fixed ratio $J/U = 1/4$ will be discussed. Around this value of J/U is where we have found the realistic AF order

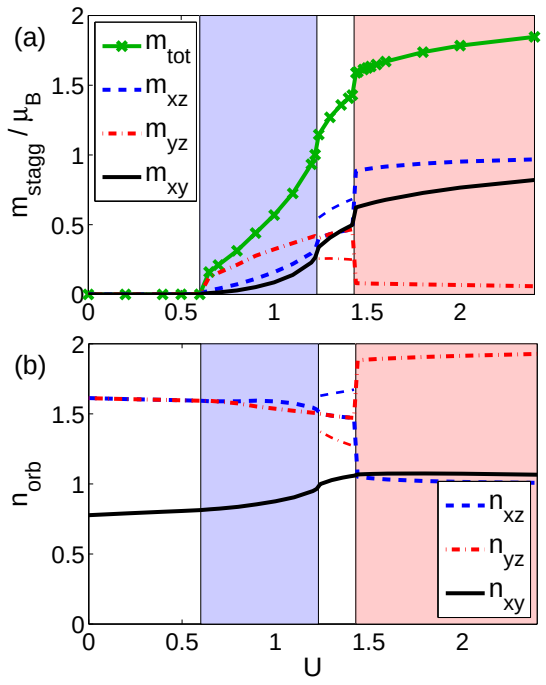

FIG. 5: (Color online) (a) Orbital magnetization and (b) occupation number as a function of the Coulomb repulsion strength U, obtained with a mean-field approximation. The colors indicate the different phases (for increasing U): uncorrelated metal, itinerant $(\pi, 0)$ antiferromagnet without orbital order, itinerant $(\pi, 0)$ antiferromagnet with alternating orbital order [small white window, spin-orbital order as in Fig. 2(h)], and a ferro-orbitally-ordered $(\pi, 0)$ antiferromagnetic insulator [spin-orbital order as in Fig. 2(a)]. Hopping parameters are from Tab. I, and $J = U/4$. For the phase with alternating orbital order, the thin lines show (a) $m \pm q$ and (b) $2n \pm p$.

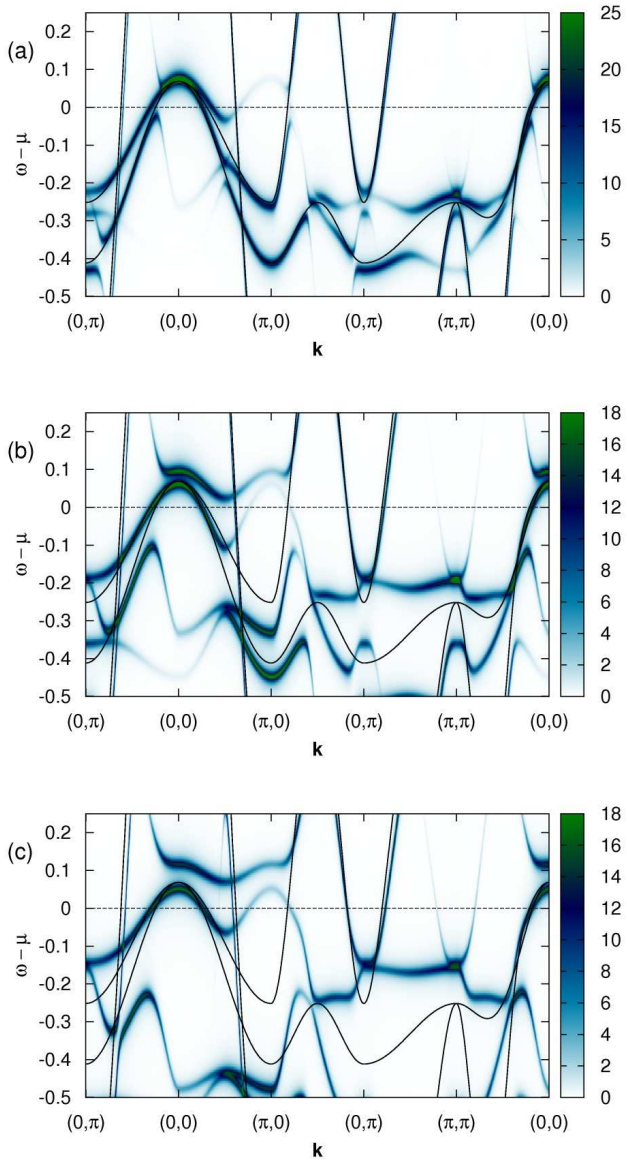

FIG. 6: (Color online) Spectral density $A(\mathbf{k}, \omega)$ for the antiferromagnet orbital-disordered metallic phase at (a) $U = 0.7$, (b) $U = 0.9$, and (c) $U = 1.1$. The BZ is for the one-Fe unit cell, and $J = U/4$ was used. The uncorrelated $A(\mathbf{k}, \omega)$ for $U = 0$ is included as solid lines for comparison.

with ordering momentum $\mathbf{q}_1 = (\pi, 0)$ for all values of $U > U_{c_1}$. Figure 5(a) shows how the staggered magnetization with ordering momentum $(\pi, 0)$ increases with the Coulomb repulsion U. As previously found for two- and four-orbital models,[25] intermediate U leads to an antiferromagnetic metal. The system remains nonmagnetic for small U up to $U_{c_1} \approx 0.6$. For $U > U_{c_1}$, the spin $(\pi, 0)$-ordered magnetic moment starts to grow, see Fig. 5(a), but the band structure remains metallic, as can be deduced from the spectral functions presented in Fig. 6, calculated for several values of the Coulomb repulsion in this regime. Note that the spin-$(\pi, 0)$ AF order triggered by U introduces gaps and magnetically-induced "shadow" bands;[62] for comparison, the uncorrelated $A(\mathbf{k}, \omega)$ is included in Fig. 6. Since several bands are involved, the gaps are not necessarily located at the chemical potential, as it has been discussed for the two- and four-orbital models in Ref. 25, and the system remains metallic. As it can be seen in Fig. 6, the overall features of the spectral density in this regime remain similar to those of the noninteracting limit, with the bandwidth being slightly reduced with increasing U. However, the onset of AF order does affect some details of $A(\mathbf{k}, \omega)$, especially low-energy features at the chemical potential, where one of the hole pockets disappears and additional pockets arise.

The Fermi surface for $U = 0.7$, where the Coulomb repulsion is just barely strong enough to induce $(\pi, 0)$ antiferromagnetism, is shown in Figs. 7(a,b). More specifically, Fig. 7(a) shows the Fermi surface in the extended BZ for spin stripes running along the y-direction, i.e., for the ordering vector $(\pi, 0)$. While the electron pocket at $(0, \pi)$ is hardly affected, the pocket at $(\pi, 0)$ has almost disappeared. Of the two hole pockets, the inner one has also disappeared for momenta $(0, k_y)$, because a gap has here developed at the chemical potential μ, see

Fig. 6(a). For momenta $(k_x, 0)$, in contrast, the gap in the *outer* pocket lies below μ, and the band consequently forms a very small electron pocket. This result is in qualitative agreement with the unconventional electronic reconstruction observed with ARPES in $(Ba, Sr)Fe_2As_2$.[63] Figure 7(b) shows the superposition of the Fermi surfaces obtained for the two equivalent ordering vectors $(\pi, 0)$ and $(0, \pi)$ in the reduced BZ corresponding to the two-Fe unit cell. If U is increased to $U = 0.9$, the gap in the outer hole pocket along $(k_x, 0)$ increases and pushes the outer band above the chemical potential; the small electron pockets seen for $U = 0.7$ in Fig. 7(a) consequently disappear, and only one hole pocket remains around Γ, see Fig. 7(c). The $(0, \pi)$ electron pocket remains unaffected, but at $(\pi, 0)$, a hole-like shadow pocket with very low spectral weight has replaced the original electron pocket. The band that formed the vanished electron pocket at $U = 0$ has been deformed strongly enough to create a small *hole*-like pocket at $\approx (\pi/2, 0)$. As it can be seen in Fig. 7(d), this hole pocket touches the $(\pi, 0)$ electron pocket once the results for ordering vectors $(\pi, 0)$ and $(0, \pi)$ are combined. As U continues to increase within the magnetic metallic phase no further qualitative changes are observed, as it can be seen in Fig. 6(c) and Fig. 7(e) and 7(f) where the spectral functions and the FS are shown for $U = 1.1$.

The average electronic occupation numbers for the three orbitals, shown in Fig. 5(b), are not significantly affected by the onset of antiferromagnetism. We believe that the small difference in electronic population observed is driven by the different orbital magnetization (see Fig. 5(a)) and is due to the orbital anisotropy relative to the direction of the magnetic $(\pi, 0)$ stripes. Note that the difference between m_{xz} and m_{yz} in Fig. 5(a) is larger than the difference between n_{xz} and n_{yz} in Fig. 5(b) indicating that q is more important than p in Eq. (13). In addition, the behavior of the spectral functions appears to be dominated by the magnetization in this phase.

When a second critical coupling $U_{c_2} \approx 1.23$ is reached, the system develops orbital order with an ordering momentum (π, π), different from the magnetic ordering vector $(\pi, 0)$; the spin-orbital order realized is the one schematically depicted in Fig. 2(h) (the order occurs between the xz and yz orbitals, i.e., $\phi = 0$.) The system remains a metal through this second transition as well, but the spectral density is profoundly affected, see Fig. 8(a). The original hole and electron pockets around Γ and M completely disappear and only correlation-induced pockets remain: the hole pocket around $\mathbf{k} = (\pi/2, 0)$ is mirrored at $\mathbf{k} \approx (\pi/2, \pi)$, and four more small pockets can be seen in the FS (not shown) away from the high-symmetry directions plotted in Fig. 8(a). Different states with different orbital ordering patterns have only slightly higher energies in this regime. In contrast, phases with different *magnetic* ordering have significantly higher energy, suggesting that the $(\pi, 0)$ AF "stripes" may be more robust than the alternating orbital order.

If U is further increased, a metal-insulator transition finally occurs at a third critical $U_{c_3} \approx 1.43$. At this point, the orbital order changes: as can be concluded from the orbital densities shown in Fig. 5(b), the system develops ferro-orbital order. The spin-$(\pi, 0)$ antiferromagnetism persists, and the spectral density in Fig. 8(b) has a full gap. The ferro-orbital spin-$(\pi, 0)$ order in this insulator is the one depicted schematically in Fig. 2(a). With growing U, the staggered magnetization converges to its maximal possible value $2\mu_{\mathrm{Bohr}}$, as shown in Fig. 5(a).

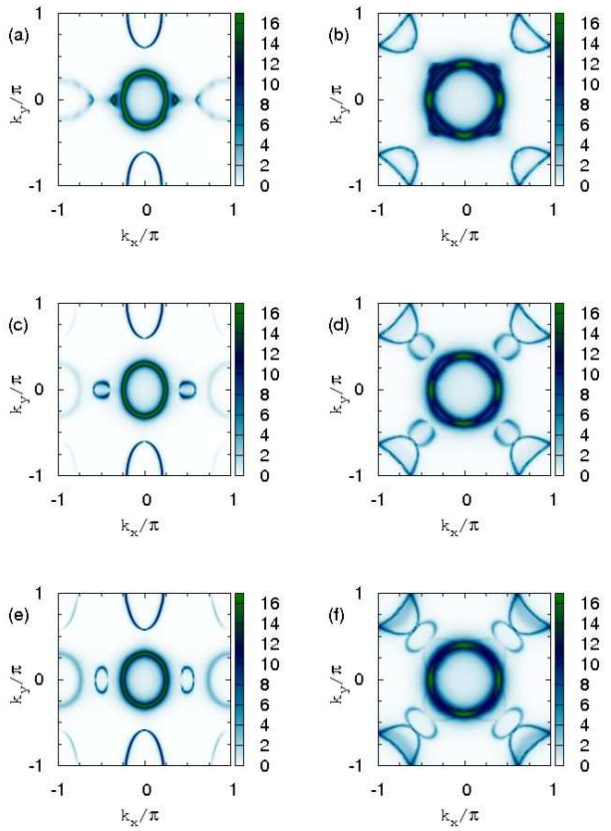

FIG. 7: (Color online) Fermi surface in the orbital-disordered spin-antiferromagnetic metallic phase with (a,b) $U = 0.7$, (c,d) $U = 0.9$, and (e,f) $U = 1.1$. (a,c,e) show the unfolded BZ containing one Fe, for the antiferromagnetic ordering vector $q = (\pi, 0)$. (b,d,f) depict the superposition of the FSs for $\mathbf{q} = (\pi, 0)$ and $\mathbf{q} = (0, \pi)$ in the (rotated) folded BZ corresponding to two Fe atoms. The ratio $J = U/4$ was used. The color scale is the same as in Fig. 6.

The direction of the magnetic stripes determines which of the two degenerate xz and yz orbitals is (almost) doubly occupied in the FO order realized at large U. For ordering vector $(\pi, 0)$ ($(0, \pi)$) it is the yz (xz) orbital. This can be understood by considering the interorbital hopping t_7 between the xy orbital and the $yz(xz)$ orbital along the y-(x-)direction, which has to be large in order to ensure xz/yz character for the hole pockets, see Sec. II B. For spin stripes along the y-direction, i.e. ordering vector $(\pi, 0)$, bonds in the x-direction are antiferromagnetic and the electrons can better take advan-

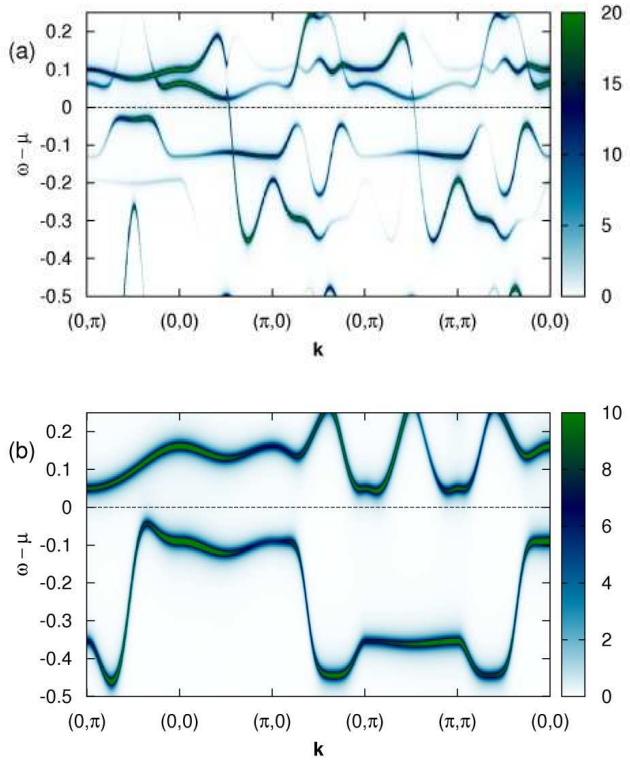

FIG. 8: (Color online) Spectral density $A(\mathbf{k},\omega)$ for (a) the orbitally-ordered spin-$(\pi,0)$ antiferromagnetic metallic phase at $U = 1.36$, and (b) the orbitally polarized spin-$(\pi,0)$ antiferromagnetic insulator at $U = 1.6$. The ratio $J = U/4$ was used, and the unfolded BZ is for the one-Fe unit cell.

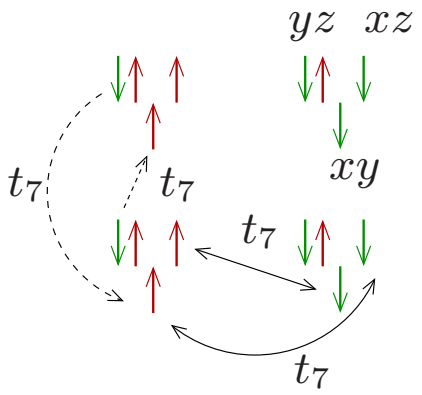

FIG. 9: (Color online) Magnetic order and orbital occupation at large U shown for four sites. The magnetic ordering vector is $(\pi,0)$, i.e, the spin stripes run along the y direction. For each site, the xy, xz, and yz orbitals are shown: the xy is the one below the other two, and the yz is doubly occupied. Dashed (continuous) lines indicate inter-orbital hopping t_7 connecting the xy orbital to xz (yz) along the x- (y-) direction.

tage of the AF superexchange if the two orbitals connected by t_7 are both singly occupied (see the schematic illustration in Fig. 9). The remaining yz orbital then has to be doubly occupied. This does not cost any AF superexchange energy, because its connection to the xy orbital via t_7 lies along the spin-aligned y-direction where such AF superexchange would in any case not occur. In fact, the additional electron in the yz orbital has the opposite spin from the majority spin of the stripes and can, thus, gain some kinetic energy by hopping via t_7 to the xy orbital along the FM y-direction. Thus, in this regime of large U the ground state corresponds to the cartoon shown in Fig. 2(a) if the magnetic order is $(\pi,0)$.

Summarizing, our mean-field calculations indicate the existence of four distinct phases that are stabilized with growing Coulomb repulsion U: (i) a disordered, paramagnetic phase for $U < U_{c_1}$, (ii) a metallic phase with $(\pi,0)$ or $(0,\pi)$ magnetic order for $U_{c_1} < U < U_{c_2}$, (iii) a metallic magnetic phase for $U_{c_2} < U < U_{c_3}$ with alternating orbital order with ordering vector (π,π), and (iv) a ferro-orbitally ordered insulator with spin-$(\pi,0)$ magnetic order for $U > U_{c_3}$, where the yz [xz] orbital has larger electronic occupation for magnetic ordering vector $(\pi,0)$ [$(0,\pi)$].

IV. PAIRING OPERATORS IN A THREE-ORBITAL MODEL FOR PNICTIDES

In this section, the spin-singlet pairing operators that are allowed by the lattice and orbital symmetries in the three-orbital model for LaOFeAs will be constructed. This classification of operators has previously been made for the two-orbital model.[64–67] An approach similar to Ref. 67 will be followed. To achieve this goal, the three-orbital tight-binding portion of the Hamiltonian, $H_{\rm TB}$, presented in Eq. (4) will be rewritten in terms of the 3×3 matrices λ_i which correspond to the eight Gell'mann matrices[68] for the cases $i = 1$ to 8, while λ_0 is the 3×3 identity (see App. B). Then, $H_{\rm TB}$ becomes

$$H_{\rm TB}(\mathbf{k}) = \sum_{\mathbf{k},\sigma} \Phi^\dagger_{\mathbf{k},\sigma} \xi_{\mathbf{k}} \Phi_{\mathbf{k},\sigma}, \tag{14}$$

where $\Phi^\dagger_{\mathbf{k},\sigma} = (d^\dagger_{xz}(\mathbf{k}), d^\dagger_{yz}(\mathbf{k}), d^\dagger_{xy}(\mathbf{k}))_\sigma$ and

$$\xi_{\mathbf{k}} = \epsilon_{\mathbf{k}}\lambda_0 + \delta_{\mathbf{k}}\lambda_3 + \gamma_{\mathbf{k}}\lambda_1 + \alpha^{(1)}_{\mathbf{k}}\lambda_5 + \alpha^{(2)}_{\mathbf{k}}\lambda_7 + h_{\mathbf{k}}\lambda_8, \tag{15}$$

with

$$\epsilon_{\mathbf{k}} = (T^{11} + T^{22} + T^{33})/3 \tag{16}$$

$$= \frac{2}{3}(t_1 + t_2 + t_5)(\cos k_x + \cos k_y) + \frac{4}{3}(2t_3 + t_6)\cos k_x \cos k_y - \mu + \frac{\Delta_{xy}}{3}, \tag{17}$$

$$\delta_{\mathbf{k}} = (T^{11} - T^{22})/2 = -(t_1 - t_2)(\cos k_x - \cos k_y), \tag{18}$$

$$\gamma_{\mathbf{k}} = T^{12} = 4t_4 \sin k_x \sin k_y, \tag{19}$$

TABLE III: Symmetry properties of the several terms in the $H_{\rm TB}$ Hamiltonian of the three-orbital model.

Term	IR
$\epsilon_{\mathbf{k}}$	A_{1g}
$\delta_{\mathbf{k}}$	B_{1g}
$\gamma_{\mathbf{k}}$	B_{2g}
$(\alpha^{(1)}_{\mathbf{k}}, \alpha^{(2)}_{\mathbf{k}})$	E_g
$h_{\mathbf{k}}$	A_{1g}

TABLE IV: Symmetry properties of Gell'mann matrices for the orbital assignment that defines the proposed three-orbital model.

Matrix	IR
λ_0	A_{1g}
λ_1	B_{2g}
λ_2	A_{2g}
λ_3	B_{1g}
(λ_4, λ_6)	E_g
(λ_5, λ_7)	E_g
λ_8	A_{1g}

$$\alpha^{(1)}_{\mathbf{k}} = T^{13}/i = -2t_7 \sin k_x - 4t_8 \sin k_x \cos k_y, \quad (20)$$

$$\alpha^{(2)}_{\mathbf{k}} = T^{23}/i = -2t_7 \sin k_y - 4t_8 \sin k_y \cos k_x, \quad (21)$$

and

$$\begin{aligned} h_{\mathbf{k}} &= \frac{T^{11}+T^{22}}{2\sqrt{3}} - \frac{T^{33}}{\sqrt{3}} \\ &= \frac{1}{\sqrt{3}}(t_1+t_2-2t_5)(\cos k_x + \cos k_y) \quad (22) \\ &\quad + \frac{4}{\sqrt{3}}(t_3-t_6)\cos k_x \cos k_y - \frac{\Delta_{xy}}{\sqrt{3}}. \end{aligned}$$

It can be shown that each element in Eqs. (15-22) transforms according to one irreducible representation of the D_{4h} group corresponding to the Fe lattice. The classification is given in Tab. III.

Since the Hamiltonian has to transform according to A_{1g}, the Gell'mann matrices in the orbital basis here chosen transform as indicated in Tab. IV.

In multiorbital systems the general form of a spin-singlet pairing operator is given by[69]

$$\Delta^\dagger(\mathbf{k}) = f(\mathbf{k})(\lambda_i)_{\alpha,\beta}(d^\dagger_{\mathbf{k},\alpha,\uparrow} d^\dagger_{-\mathbf{k},\beta,\downarrow} - d^\dagger_{\mathbf{k},\beta,\uparrow} d^\dagger_{-\mathbf{k},\alpha,\downarrow}), \quad (23)$$

where a sum over repeated indices is implied; the operators $d^\dagger_{\mathbf{k},\alpha,\sigma}$ have been defined in the previous sections and $f(\mathbf{k})$ is the form factor that transforms according to one of the irreducible representations of the crystal's symmetry group. Although $f(\mathbf{k})$ may, in general, have a very complicated form, a short pair-coherence length requires the two electrons that form the pair to be very close to each other. Consequently, for simplicity we focus on nearest and diagonal next-nearest neighbors, and form factors that are allowed in a lattice with D_{4h} symmetry. The momentum dependent expression, as well as the irreducible representation according to which each form factor transforms, are given in Tab. V. Note that if the pairing mechanism is non-BCS and if the Coulomb repulsion is strong on-site pairing, then f(k)=1 corresponding to onsite pairing is an unlikely factor.

TABLE V: Form factors $f(\mathbf{k})$ for pairs up to distance (1,1) classified according to their symmetry under D_{4h} operations.

#	$f(\mathbf{k})$	IR
1	1	A_{1g}
2	$\cos k_x + \cos k_y$	A_{1g}
3	$\cos k_x \cos k_y$	A_{1g}
4	$\cos k_x - \cos k_y$	B_{1g}
5	$\sin k_x \sin k_y$	B_{2g}
6	$(\sin k_x, \sin k_y)$	E_g
7	$(\sin k_x \cos k_y, \sin k_y \cos k_x)$	E_g

TABLE VI: Product table for the irreducible representations of the group D_{4h} relevant to this work.

	A_{1g}	A_{2g}	B_{1g}	B_{2g}	E_g
A_{1g}	A_{1g}	A_{2g}	B_{1g}	B_{2g}	E_g
A_{2g}	A_{2g}	A_{1g}	B_{2g}	B_{1g}	E_g
B_{1g}	B_{1g}	B_{2g}	A_{1g}	A_{2g}	E_g
B_{2g}	B_{2g}	B_{1g}	A_{2g}	A_{1g}	E_g
E_g	E_g	E_g	E_g	E_g	$A_{1g}+A_{2g}+B_{1g}+B_{2g}$

A. Intraorbital Pairing

The previous discussion shows that the symmetry of the pairing operator will be exclusively determined by the symmetry of $f(\mathbf{k})$ *only* if λ_i transforms according to A_{1g}. Table IV indicates that this is the case for pairing operators constructed by using λ_0 or λ_8 in Eq. (23). These two matrices are diagonal, which means that such pairing operators define *intraorbital* pairings. For intraorbital pairing, with a symmetry fully determined by the spatial form factor, the basis functions are then given by: #I:$f(\mathbf{k})\lambda_0$ or #II: $f(\mathbf{k})\lambda_8$.

For #I, the superconducting order parameter (OP) will be the same for the three orbitals while #II allows the OP for xy to be different than for xz and yz which need, by symmetry, to have OPs that can only differ by a relative sign. Thus, the addition of a third orbital may allow the possibility of different superconducting gaps in the band representation, reminiscent of the two gaps in MgB_2.[70,71]

When any of the remaining seven matrices λ_i appear in Eq. (23), the symmetry of the pairing operator is given by the irreducible representation of D_{4h} resulting from the product of the symmetry of the form factor and the symmetry of the orbital component,[69] according to the product table given in Tab. VI. For $\lambda_i = \lambda_3$, the basis function is given by #III: $f(\mathbf{k})\lambda_3$. The pairing is still intraorbital but since λ_3 transforms according to B_{1g} the symmetry of the operator will be B_{1g} if $f(\mathbf{k})$ transforms according to A_{1g}, etc. Note that this pairing operator does not involve the xy orbital and it has already been

presented in the context of the two-orbital model.[67] However, since the orbital composition of the bands is not the same as for the two-orbital model, it will be important to determine whether the gap structure of this pairing operator has changed.

B. Interorbital Pairing

The remaining six λ_i matrices lead to interorbital pairing. Note that λ_1 and λ_2 do not involve the orbital xy and the pairing operators that they generate have already been discussed in the two-orbital model.[67] We are interested in the spin-singlet pairing operator for orbitals xz/yz that has a basis #IV:$f(\mathbf{k})\lambda_1$. This operator, with $f(\mathbf{k}) = \cos k_x + \cos k_y$, has been found to be favored for intermediate values of the Coulomb repulsion U in numerical calculations of the two-orbital model for pnictides.[23,24] The addition of the xy orbital leads to the possibility of new interorbital pairing operators, i.e., pairing between electrons in the orbitals xz and yz with electrons in the xy orbital. Thus, now the focus will be on the interorbital spin-singlet pairing operators that result from the addition of xy.

The interorbital case becomes very interesting because we need to combine (xz,yz) that transform as the two-dimensional representation E_g with xy that transforms as B_{2g}; thus, the product transforms as E_g. The λ_i matrices that can appear in this intraorbital pairing are (λ_4, λ_6) or (λ_5, λ_7). Since the focus here is on pairing operators that are spin singlets, it will be required that the operator is even under orbital exchange. Thus, only (λ_4, λ_6) will be considered since the other two matrices (λ_5, λ_7) that transform according to E_g will produce operators odd under orbital exchange. Let us further restrict the analysis to the case of pairing operators that transform according to one dimensional representations of the point group because we assume that the ground state is non degenerate. Thus, the only spatial form factors $f(\mathbf{k})$ that we should consider must transform according to E_g. This leaves us with

$$f(\mathbf{k}) = (\sin k_x, \sin k_y), \tag{24}$$

for nearest neighbor pairs and

$$f(\mathbf{k}) = (\sin k_x \cos k_y, \cos k_x \sin k_y), \tag{25}$$

for diagonal pairs. Since the direct product of two E_g representations is $E_g \times E_g = A_{1g} + A_{2g} + B_{1g} + B_{2g}$, pairing operators transforming according to four irreducible representations will be obtained. The basis for the new pairing operators, labeled V_i, are presented in Tab. VII.

C. Band Representation

To obtain the gap structure of the pairing operators #I to #IV (shown in Table VII) the Bogoliubov-de Gennes Hamiltonian (BdG) is constructed and it is given by

$$H_{\mathrm{BdG}} = \sum_{\mathbf{k}} \Psi_{\mathbf{k}}^{\dagger} H_{\mathbf{k}}^{\mathrm{MF}} \Psi_{\mathbf{k}}, \tag{26}$$

with the definitions

$$\begin{aligned} \Psi_{\mathbf{k}}^{\dagger} = (&d_{\mathbf{k},xz,\uparrow}^{\dagger}, d_{\mathbf{k},yz,\uparrow}^{\dagger}, d_{\mathbf{k},xy,\uparrow}^{\dagger}, \\ &d_{-\mathbf{k},xz,\downarrow}, d_{-\mathbf{k},yz,\downarrow}, d_{-\mathbf{k},xy,\downarrow}), \end{aligned} \tag{27}$$

and

$$H_{\mathbf{k}}^{\mathrm{MF}} = \begin{pmatrix} H_{\mathrm{TB}}(\mathbf{k}) & P(\mathbf{k}) \\ P^{\dagger}(\mathbf{k}) & -H_{\mathrm{TB}}(\mathbf{k}) \end{pmatrix}, \tag{28}$$

where each element represents a 3×3 block with $H_{\mathrm{TB}}(\mathbf{k})$ given by Eq. (4) and

$$P(\mathbf{k})_{\alpha,\beta} = V f(\mathbf{k}) (\lambda_i)_{\alpha,\beta}, \tag{29}$$

with $i = 0$, 8, 3, and 1 for pairing #I, #II, #III, and #IV, respectively. V is the magnitude of the OP given by the product of the pairing attraction V_0 and a mean-field parameter Δ that should be obtained from minimization of the total energy.[69] For pairing #V_i the basis listed in Table VII should be used instead of $f(\mathbf{k})\lambda_i$.

Up to this point we have worked using the orbital representation because this basis renders it straightforward to obtain the form of the Hamiltonian, as well as the pairing operators allowed by the symmetry of the lattice and orbitals. However, the experimentally observed superconducting gaps occur at the FS determined by the bands that result from the hybridization of the orbitals. For this reason, it is convenient to express Eq. (28) in the band representation. $H_{\mathrm{TB}}(\mathbf{k})$ can be expressed in the band representation via the transformation $H_{\mathrm{Band}}(\mathbf{k}) = U^{\dagger}(\mathbf{k}) H_{\mathrm{TB}}(\mathbf{k}) U(\mathbf{k})$, where $U(\mathbf{k})$ is the unitary change of basis matrix and $U^{\dagger}(\mathbf{k})$ is the transpose conjugate of $U(\mathbf{k})$. Since U is unitary it is known that for each value of $\mathbf{k}$, $\sum_i (U_{i,j})^* U_{i,k} = \sum_i (U_{j,i})^* U_{k,i} = \delta_{j,k}$. Then, $H'_{\mathrm{MF}} = G^{\dagger} H_{\mathrm{MF}} G$ where G is the 6×6 unitary matrix composed of two 3×3 blocks given by U. Then,

$$H_{\mathbf{k}}^{\prime \mathrm{MF}} = \begin{pmatrix} H_{\mathrm{Band}}(\mathbf{k}) & P_B(\mathbf{k}) \\ P_B^{\dagger}(\mathbf{k}) & -H_{\mathrm{Band}}(\mathbf{k}) \end{pmatrix}, \tag{30}$$

TABLE VII: Properties of pairing operators in the three-orbital model. f indicates the symmetry of $f(\mathbf{k})$.

No.	IR	Basis	Gap
I	f	$f(\mathbf{k})\lambda_0$	Full or Nodal
II	f	$f(\mathbf{k})\lambda_8$	Full or Nodal
III	fB_{1g}	$f(\mathbf{k})\lambda_3$	Nodal
IV	fB_{2g}	$f(\mathbf{k})\lambda_1$	Nodal
V_a	A_{1g}	$\sin k_x \lambda_4 + \sin k_y \lambda_6$	Nodal
V_b	A_{1g}	$\lambda_4 \sin k_x \cos k_y + \lambda_6 \cos k_x \sin k_y$	Nodal
V_c	B_{1g}	$\sin k_x \lambda_4 - \sin k_y \lambda_6$	Nodal
V_d	B_{1g}	$\lambda_4 \sin k_x \cos k_y - \lambda_6 \cos k_x \sin k_y$	Nodal
V_e	A_{2g}	$\sin k_x \lambda_6 + \sin k_y \lambda_4$	Nodal
V_f	A_{2g}	$\lambda_4 \cos k_x \sin k_y + \lambda_6 \sin k_x \cos k_y$	Nodal
V_g	B_{2g}	$\sin k_x \lambda_6 - \sin k_y \lambda_4$	Nodal
V_h	B_{2g}	$\lambda_4 \cos k_x \sin k_y - \lambda_6 \sin k_x \cos k_y$	Nodal

with

$$P_B(\mathbf{k}) = U^{-1}(\mathbf{k})P(\mathbf{k})U(\mathbf{k}). \tag{31}$$

A standard assumption in superconducting multiband systems is that the pairing interaction should be purely intraband, meaning that $P_B(\mathbf{k})$ is diagonal. Thus, let us explore what kind of purely intraband pairing operators are allowed by the symmetry properties of the three-orbital model for LaOFeAs. In the band representation, the most general BdG matrix with purely intraband pairing is given by

$$H'_{\rm MF} = \begin{pmatrix} \epsilon_1(\mathbf{k}) & 0 & 0 & \Delta_1(\mathbf{k}) & 0 & 0 \\ 0 & \epsilon_2(\mathbf{k}) & 0 & 0 & \Delta_2(\mathbf{k}) & 0 \\ 0 & 0 & \epsilon_3(\mathbf{k}) & 0 & 0 & \Delta_3(\mathbf{k}) \\ \Delta_1^*(\mathbf{k}) & 0 & 0 & -\epsilon_1(\mathbf{k}) & 0 & 0 \\ 0 & \Delta_2^*(\mathbf{k}) & 0 & 0 & -\epsilon_2(\mathbf{k}) & 0 \\ 0 & 0 & \Delta_3^*(\mathbf{k}) & 0 & 0 & -\epsilon_3(\mathbf{k}) \end{pmatrix}, \tag{32}$$

where $\epsilon_i(\mathbf{k})$ are the eigenvalues of $H_{\rm TB}(\mathbf{k})$ and $\Delta_i(\mathbf{k})$ denotes the band and momentum dependent pairing interactions.[72] As it can be deduced from the properties of the unitary change of basis matrix U, if all three bands have the same pairing interaction, i.e. $\Delta_1(\mathbf{k}) = \Delta_2(\mathbf{k}) = \Delta_3(\mathbf{k}) = \Delta(\mathbf{k})$, then the matrix $P(\mathbf{k})$ in the orbital representation will also be diagonal. In this case, the pairing operator is given by Eq. (23) with an arbitrary $f(\mathbf{k})$ and $\lambda_i = \lambda_0$, i.e., the pairing operator is intraorbital and the OP is the same for the three orbitals. This corresponds to pairing operator #I which describes a pairing interaction that is the *same* for each of the three orbitals. However, symmetry only requires that the orbitals xz and yz must have the same OP, while xy can have a different one. Thus, there does not seem to be a reason to assume that electrons in the many bands that determine the FS should be affected by the same pairing interactions. In fact, in MgB_2 the electron-phonon interaction that provides the pairing is stronger on the σ-bands than on the π-bands giving, as a result, two different superconducting gaps. Thus, it can be asked whether the symmetry of the three-orbital model allows for the possibility of two different OPs with a pure intraband pairing interaction. If it is assumed that in Eq.(32) $\Delta_1 = \Delta_2 = \Delta = f(\mathbf{k})C$ and $\Delta_3 = \Delta' = f(\mathbf{k})C'$, then in the orbital representation

$$P(\mathbf{k})_{\alpha,\beta} = U_{\alpha,3}(\mathbf{k})U^*_{\beta,3}(\mathbf{k})f(\mathbf{k})(C' - C), \tag{33}$$

for the off-diagonal elements and

$$P(\mathbf{k})_{\alpha,\alpha} = \Delta + |U_{\alpha,3}(\mathbf{k})|^2 f(\mathbf{k})(C' - C), \tag{34}$$

for the diagonal ones.

Now let us concentrate on the diagonal part. This has to arise from a linear combination of intraorbital pairing operators with compatible symmetries. There are two possibilities:

$$P(\mathbf{k})_{\alpha,\alpha} = f(\mathbf{k})[A(\lambda_0)_{\alpha,\alpha} + B(\lambda_8)_{\alpha,\alpha}], \tag{35}$$

or

$$P(\mathbf{k})_{\alpha,\alpha} = Df(\mathbf{k})(\lambda_3)_{\alpha,\alpha}, \tag{36}$$

where A, B, and D are independent of momentum. It can be shown that Eq. (35) requires $|U_{13}|^2 = |U_{23}|^2$ while Eq. (36) requires $|U_{13}|^2 = -|U_{23}|^2$, which are not satisfied by the elements of the matrix U determining the change of basis. This means that any purely intraband pairing interaction allowed by the symmetry of the three-orbital model should be the same for the three bands. On the other hand, if we had a case in which $|U_{13}|^2 = |U_{23}|^2 = 0$, which means that one of the three orbitals does not hybridize with the other two, it would be possible to have a system with two different gaps. Note that this is the situation for MgB_2 in which the z orbital that forms the π band does not hybridize with the x and y orbitals that constitute the σ band.

Summarizing, it has been found that independent gaps in different Fermi surfaces cannot arise if the hybridization among all the orbitals is strong and the pairing interaction is purely intraband.

D. The $s\pm$ Pairing Operator

The next issue to be considered is whether the orbital and lattice symmetries allow for the possibility of the often discussed $s\pm$ pairing scenario. ARPES experiments indicate the existence of two hole-pockets around Γ. The interior pocket, which is almost nested with the electron pockets with a nesting vector $\mathbf{q} = (\pi, 0)$ or $(0, \pi)$, develops a constant gap Δ_h which has the same magnitude than the gap on the electron pockets Δ_e. In addition, they find a smaller gap $\Delta'_h \approx \Delta_h/2$ on the exterior hole pocket.[47] The ARPES results can be interpreted in two different ways in the context of a three-orbital model:

(i) Assume that the inner hole pocket observed in ARPES corresponds to two almost degenerate FS that cannot be resolved, and assign the external hole pocket to a band that arises when extra orbitals are added. This is the same assumption made in the two-orbital model for which it was shown in Ref. 24 that the $s\pm$ pairing state is compatible with the lattice and orbital symmetries.

Under this assumption, in the three-orbital model the $s\pm$ pairing state corresponds to our pairing operator #I with $f(\mathbf{k}) = \cos k_x \cos k_y$, which in the band representation leads to a purely intraband pairing attraction given by $\Delta_i(\mathbf{k}) = V \cos k_x \cos k_y$ for each of the three-bands. For hole pockets almost degenerate with each other, the gap in both bands will be the same and there will be a sign difference with the gap at the electron pockets whose Fermi momentum differs from those of the hole pockets by $(0, \pi)$ or $(\pi, 0)$.

(ii) Assume that the inner and outer hole pockets observed by ARPES are described by the two hole pockets in the three-orbital model. This would force us to request that, for example, $\Delta_1(\mathbf{k}) = -\Delta_3(\mathbf{k} + \mathbf{q})$ where $\mathbf{q} = (\pi, 0)$ or $(0, \pi)$ and $\Delta_2(\mathbf{k})$ is independent. Then, let

us assume that $\Delta_1(\mathbf{k}) = \Delta_3(\mathbf{k}) = \cos k_x \cos k_y \Delta_0$ and $\Delta_2(\mathbf{k}) = \Delta(\mathbf{k})$. Let us concentrate on the Γ-X direction. Along this direction, $\gamma_{\mathbf{k}}$ and $\alpha^{(i)}_{\mathbf{k}}$ vanish, meaning that there is no hybridization among the three orbitals. From Fig. 1 we observe that each of the two hole FS results from the crossing of xz and yz, while the electron FS has pure xy character. From the orbital symmetry, then, it is deduced that the only reason for having different gaps at the two hole-like FS would be a strong momentum dependence of the gap since symmetry enforces $|\Delta_{xz}(\mathbf{k})| = |\Delta_{yz}(\mathbf{k})|$; in addition, the gap at the electron pockets does not need to be related to the gap in the hole pockets, unless the pairing operator contains λ_0. Thus, we observe that the $s\pm$ pairing operator could be supported under this assumption if it is given by Eq. (23) with $f(\mathbf{k}) = \cos k_x \cos k_y$ with $\lambda_i = \lambda_0$ and the additional condition that if $\mathbf{k}^{FS_h}$ represents the Fermi momentum of the internal hole pocket and $\mathbf{k}^{FS_{h'}} = \mathbf{k}^{FS_h} + \delta$ is the Fermi momentum of the external hole pocket it is necessary that $f(\mathbf{k}^{FS_h})/f(\mathbf{k}^{FS_{h'}}) \approx 2$ which would require fine tuning of the parameters. It would also be expected that in this scenario the ratio $\Delta_{h'}/\Delta_h$ should not be 1/2 for all materials.

Thus, it is concluded that the $s\pm$ pairing could be supported by a three-orbital model. It corresponds to pairs of electrons in the same orbital at distance one along the diagonals of the square lattice, i.e., on next-nearest neighbor sites, with the same pairing potential for all three orbitals. Then, if experiments show that $s\pm$ is indeed the correct pairing operator, it will remain to be understood why the pairing interaction does not appear to depend on the symmetry of each different orbital or, equivalently, why it is the same for electrons in different bands. This should be contrasted with the case of MgB_2 in which the strength of the electron-phonon coupling that leads to pairing is stronger on the σ-band FS than in the π-band FS.

Since the pairing mechanism for the pnictides is not known and the $s\pm$ pairing state is just one of many proposed states, our discussion will continue by analyzing the other new pairing states that are allowed by symmetry when the xy orbital is considered.

E. Properties of the Pairing Operators

In the previous subsection, it was shown that only pairing #I can lead to a purely intraband pairing interaction in the context of the three-orbital model, and that the widely proposed $s\pm$ pairing state indeed belongs to the class represented by pairing #I. On the other hand, given the complexity of the problem, only numerical simulations can clarify whether the three-orbital model becomes superconducting upon doping and what is the symmetry of the dominant pairing state. Since numerical results are not yet available, here the properties of the other possible spin singlet pairing operators will be discussed.

Let us start with pairing #II, i.e. the intraorbital pairing operator containing λ_8, that allows a different pairing strength for the xy orbital. This pairing operator is not purely intraband. This fact can be easily deduced from the properties of the unitary change of basis matrices. In this case, $P(\mathbf{k})_{\alpha,\beta} = C_\alpha \delta_{\alpha\beta}$ with $C_1 = C_2 = Vf(\mathbf{k})/\sqrt{3}$ corresponding to orbitals xz and yz, and $C_3 = -2Vf(\mathbf{k})/\sqrt{3}$ for orbital xy. Then,

$$P_B(\mathbf{k})_{\alpha,\beta} = \sum_i C_i U^*_{i,\alpha}(\mathbf{k}) U_{i,\beta}(\mathbf{k}), \tag{37}$$

which does not vanish for all values of $\mathbf{k}$ for $\alpha \neq \beta$, thus indicating the existence of interband pairing terms. Similar calculations for all the pairing operators presented in Table VII show nonvanishing interband pairing terms.

Then, it is concluded that starting from the orbital representation, the only way to obtain pure intraband pairing in the band representation is by considering a pairing interaction that affects equally all the orbitals involved, producing equal gaps in all the orbitals and/or bands with symmetry determined by the spatial form factor. This shows that the requirement of purely intraband pairing induces a strong constraint regarding the coupling of the electrons in the different orbitals with the source of the pairing attraction. On the other hand, if the requirement is relaxed, interband pairing occurs at least in some regions of the BZ.[69] It was verified that this is the case for the remaining operators #II, #III, #IV, and #V$_i$. It has also been observed, by monitoring the eigenvalues of $H_{\rm BdG}$ for operators #III and #IV, that there is a nodal structure in the superconducting gap for all the values of $f(\mathbf{k})$ shown in Tab. V, while operator #II becomes nodeless for $f(\mathbf{k}) = \cos k_x \cos k_y$ or 1 at a finite value of V. In addition, some linear combinations of pairing #I and #II with $f(\mathbf{k}) = \cos k_x \cos k_y$ or 1 are also nodeless for all finite values of V but they lead to interband pairing interactions. These nodeless states that we call s_{IB} will be discussed in Sec.IV E 2.

1. *Pairing with Pseudocrystal Momentum* $\mathbf{Q} = (\pi, \pi)$

In Sec. II B, it was explained that although the three-orbital Hamiltonian retains the two-iron unit cell of the original FeAs planes, it is possible to express it in terms of three orbitals in the space of pseudocrystal momentum $\mathbf{k}$ defined in the extended Brillouin zone corresponding to a base with one single Fe atom per unit cell. In terms of the real momentum, the Hamiltonian consists of two 3×3 blocks $H_1(\mathbf{k})$ and $H_2(\mathbf{k})$ with $H_1(\mathbf{k}) = H_{\rm TB}(\mathbf{k}) = H_2(\mathbf{k} + \mathbf{Q})$; thus, these two blocks provide the same eigenvalues in the unfolded Brillouin zone, but both blocks need to be considered if the actual reduced BZ is used. This means that in the reduced BZ the bands arise as combinations of six orbitals labeled by the orbital index $\alpha = 1$, 2, or 3, and the Hamiltonian block index $i = 1$ or 2. Then, to consider all the possible interorbital pairing operators it is important to include

pairs formed by electrons in orbitals in the two different blocks. In the extended BZ, this is equivalent to considering pairs with both pseudocrystal momentum 0 and $\mathbf{Q}$. Note that Cooper pairs with pseudocrystal momentum $\mathbf{Q}$ still have zero center-of-mass momentum. Exact diagonalization studies of the two-orbital model[23,24] did not favor such operators, and it is possible that this kind of pairing does not occur in the three-orbital model either. However, since symmetry allows such a possibility, pairing operators with nonzero pseudocrystal momentum will here be discussed for completeness.

The generalized Bogoliubov-de Gennes matrix $H^{\rm MF}_{\mathbf{k}}$ that allows us to consider interorbital pairs with pseudocrystal momentum $\mathbf{Q}$ is given by:

$$H^{\rm MF}_{\mathbf{k}}=\begin{pmatrix} H_{\rm TB}(\mathbf{k}) & 0 & 0 & P(\mathbf{k}) \\ 0 & -H_{\rm TB}(\mathbf{k}) & P(\mathbf{k}+\mathbf{Q}) & 0 \\ 0 & P^{\dagger}(\mathbf{k}+\mathbf{Q}) & H_{\rm TB}(\mathbf{k}+\mathbf{Q}) & 0 \\ P^{\dagger}(\mathbf{k}) & 0 & 0 & -H_{\rm TB}(\mathbf{k}+\mathbf{Q}) \end{pmatrix}, \tag{38}$$

where $P(\mathbf{k})$ has the form given in Eq. (29).

By finding the eigenvalues of $H^{\rm MF}_{\mathbf{k}}$, the structure of the gap of the possible pairing operators with pseudocrystal momentum $\mathbf{Q}$ can be obtained. Our analysis shows that all the pairing operators with pseudocrystal momentum $\mathbf{Q}$ lead to inter and intraband pairing in the band representation and nodes on the FS for small V. We have observed that a nodeless gap for pairs with pseudocrystal momentum $\mathbf{Q}$ develops at a finite value of V for operators #I and #II with $f(\mathbf{k}) = 1$ or $\cos k_x \cos k_y$ in a manner characteristic of systems with interband pairing.[69]

2. *Spectral Functions*

It is straightforward to calculate the spectral functions $A(\mathbf{k},\omega)$ for all the pairing operators presented in this manuscript. However, due to their large number, we will concentrate on *(i)* pairing operator #I with $f(\mathbf{k}) = \cos k_x \cos k_y$, i.e., the $s\pm$ pairing operator, *(ii)* a linear combination of pairing operators #I and #II with $f(\mathbf{k}) = \cos k_x \cos k_y$, that we will call the s_{IB} pairing operator; *(iii)* pairing operator #IV with $f(\mathbf{k}) = \cos k_x + \cos k_y$, i.e., the B_{2g} pairing operator, favored by numerical calculations in the magnetic metallic regime of the two-orbital model, which will be called B_{2g}, and *(iv)* a linear combination of pairing operator #IV with $f(\mathbf{k}) = \cos k_x + \cos k_y$ and pairing operator $\#V_g$ with pseudocrystal momentum $\mathbf{Q}$, which is the natural extension to three orbitals of B_{2g} and will be called $B^{\rm ext}_{2g}$.

In Fig. 10(a) the spectral functions $A(\mathbf{k},\omega)$ along high symmetry directions in the reduced Brillouin zone are shown for the three-orbital Hamiltonian with $V = 0$, i.e., without pairing, in order to illustrate the changes induced by the various pairing interactions considered here. Note that these results correspond to the system with two Fe atoms per unit cell, which leads to the six bands seen in Fig. 10(a). The results for the $s\pm$ pairing operator

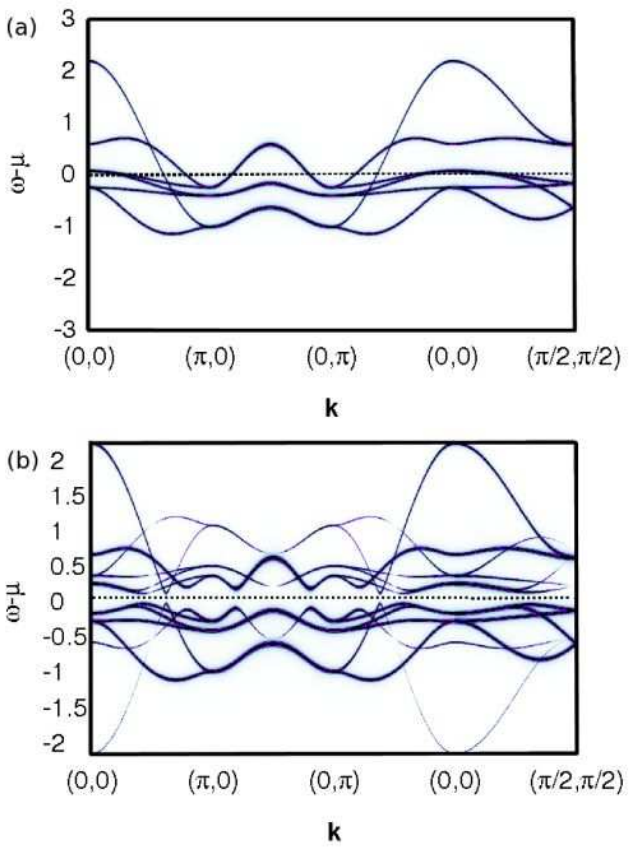

FIG. 10: (Color online) The intensity of the points represents the values of the spectral function $A(\mathbf{k},\omega)$ for the three-orbital model with pairing interaction (a) $V = 0$; (b) $V = 0.2$, for the $s\pm$ pairing operator given in the text.

with intensity $V = 0.2$ are presented in Fig. 10(b). It can be observed that a gap opens at the FS and shadow Bogoliubov bands, which should be visible in ARPES experiments, appear. Numerically, we have verified that no nodes occur anywhere in the BZ. Note that the gap is momentum dependent because $f(\mathbf{k}) = \cos k_x \cos k_y$. This means that the ratio between the gaps at the FS is determined by $|f(\mathbf{k}_i)/f(\mathbf{k}_j)|$, where i and j can take the values 1, 2, 3 corresponding to the three bands that determine the FS, i.e., 1 (2) for the interior (exterior) hole pocket, and 3 for the electron pockets. This creates a constraint on how different these gaps can be if $s\pm$ represents the actual pairing symmetry of the pnictides.

As previously mentioned, we can define a pairing operator s_{IB} by combining operators #I and #II with $f(\mathbf{k}) = \cos k_x \cos k_y$ so that the orbital part of the basis is given by $A\lambda_0 + B\lambda_8$, where A and B are constants. This pairing operator is diagonal in the orbital representation, and transforms according to A_{1g} thus, it has S symmetry; it also has intra and interband terms in the band representation. This is why this operator is called s_{IB}. For a robust range of values of A and B, a nodeless gap opens on all FSs for any finite value of V. For example, we can choose the parameters in such a way that

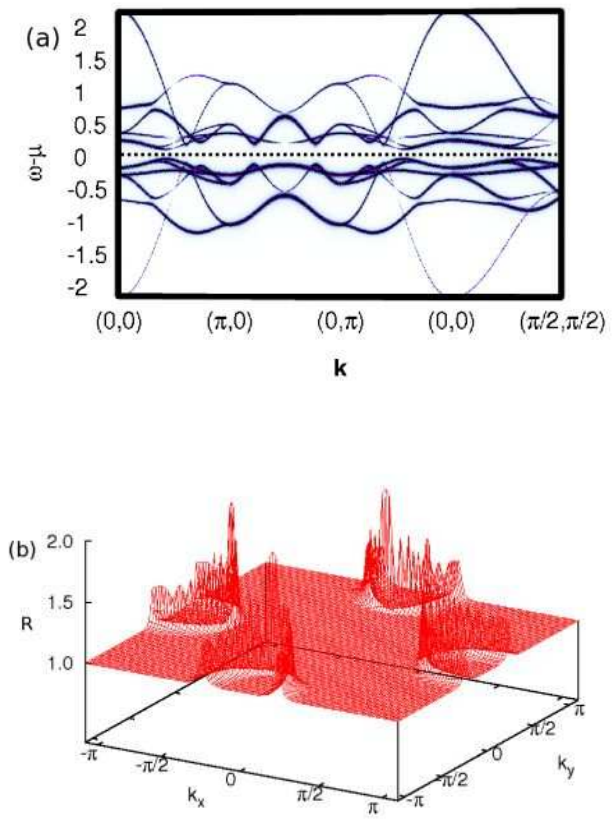

FIG. 11: (Color online) (a) The intensity of the points represents the values of the spectral function $A(\mathbf{k},\omega)$ for the three-orbital model with pairing interaction $V = 0.2$ for the pairing state s_{IB} along the indicated high symmetry directions in the folded BZ. (b) Ratio R between the gaps for pairing s_{IB} and pairing $s\pm$ for $V = 0.05$ in the unfolded BZ.

for any given $\mathbf{k}$, the pairings for the three orbitals have the same sign. The spectral functions for $V = 0.2$ along high symmetry directions in momentum space are shown in Fig. 11(a) for the special case in which $A = 3/2$ and $B = -\sqrt{3}/2$. The major difference with the results for the $s\pm$ state [see Fig. 10(b)] is that the interband pairing present in s_{IB} opens gaps between the bands away from the FS. This is a feature that should be observed in ARPES experiments. Also the band spectral functions in both cases are very different close to $(0,\pi)$ and $(\pi,0)$.

We have also investigated how the gaps on the different FSs differ for pairing $s\pm$ and s_{IB}. In Fig. 11(b) we show the ratio R between the two gaps in the unfolded BZ for $V = 0.05$. It can be seen that on the hole pockets $R = 1$, but an appreciable difference is observed on the electron pockets where $R = 2$ at the point where the electron pocket is entirely formed by xy, and diminishes as the hybridization of xy with xz or yz becomes stronger. The maximum value of R is a function of the values of A and B in the linear combination that defines s_{IB}. Thus, while $s\pm$ is characterized by gaps with a weak momentum dependence and with similar magnitudes on the hole and electron pockets, the s_{IB} state is characterized by a different gap on the electron pockets with stronger momentum dependence due to the hybridization.

Now we focus on the spectral function for operator B_{2g} presented in Fig. 12(a). This is the pairing operator that was favored by numerical calculations in the intermediate U regime of the two-orbital model and it only pairs electrons in orbital xz with electrons in orbital yz.[24] Although neither this pairing operator nor the Fermi surfaces defining the two hole pockets involve the xy orbital, the results around the hole pockets differ in the two- and three-orbital models. In the latter, much lower values of the pairing attraction V are sufficient to remove the extra nodes found close to the hole-pocket FS along the Γ-$X(Y)$ directions in the two-orbital model. This happens because the bands forming the two hole pockets are now degenerate at Γ and the pockets are consequently at almost the same momenta of the extended BZ, while they were separated by (π,π) in the two-band model. As a result, a small interorbital pairing can now overcome the separation between the two FSs and induce a full gap at the hole pockets.[69] At the electron pockets a third node, in addition to the two of the two-orbital model, is found along the Γ-$X(Y)$ direction, where the pocket has purely xy character and is, thus, not affected by the operator B_{2g}. Thus, this pairing operator would show full gaps on the hole pocket FS and nodal gaps on the electron pocket FS.

Figure 12(b) shows the spectral functions for pairing operator $B_{2g}^{\rm ext}$, which is a linear combination of B_{2g} with the pairing operator V_g (with crystal momentum $\mathbf{Q}$), i.e. next-nearest-neighbor interorbital pairing among electrons in all three orbitals is allowed. We find that nodes occur only at the electron pockets. As V increases, nodes at the electron pockets remain only along the Γ-$X(Y)$ directions because one of the electron pockets is formed by a non-hybridized orbital xy along this direction, and the relevant pairing interaction is zero for the Fermi momentum. We also investigated $A(\mathbf{k},\omega)$ for a similarly extended B_{1g} pairing $B_{1g}^{\rm ext} = (\cos k_x + \cos k_y)\lambda_3 - a(\cos k_x - \cos k_y)(\lambda_0 - \sqrt{3}\lambda_8)/3$ (not shown), which is nodal for extremely small V, with nodes in the Γ-M direction on the hole pockets, but where the nodes are already lifted for finite but small $V \gtrsim 0.01$ for many non-zero values of a.

Summarizing, we have found that among the nearest and next-nearest neighbor pairing operators allowed by symmetry only the $s\pm$ pairing operator is purely intraband and produces nodeless gaps for all values of the pairing attraction V. Thus, purely intraband pairing interactions occur only if electrons in each of the three orbitals are subjected to the same pairing attraction, i.e. when the identity matrix λ_0 characterizes the orbital portion of the pairing operator. We also found that some linear combinations of pairing operators #I and #II produce nodeless gaps for any finite V if $f(\mathbf{k}) = \cos k_x \cos k_y$, but interband attraction appears in parts of the BZ. Finally,

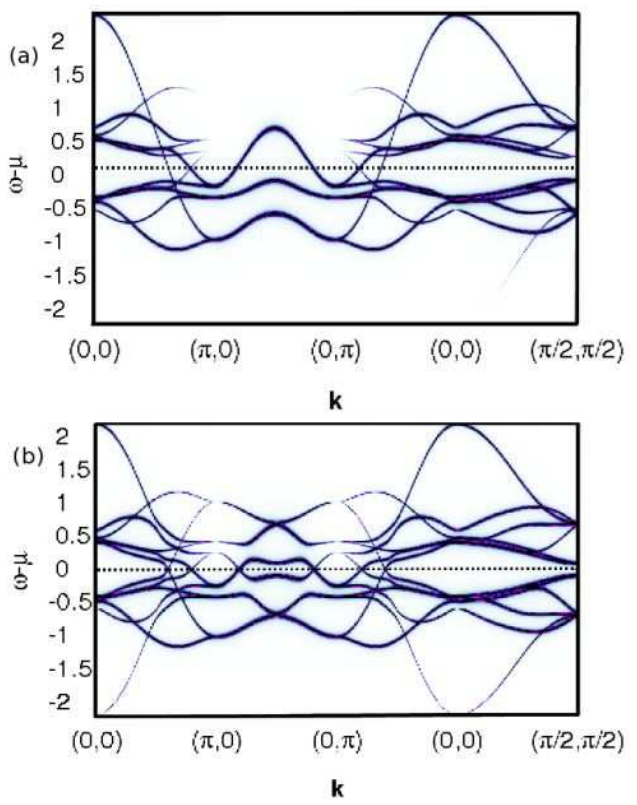

FIG. 12: (Color online) The intensity of the points represent the values of the spectral function $A(\mathbf{k},\omega)$ for the three-orbital model with the pairing interaction $V = 0.2$, for the pairing operators (a) B_{2g} and (b) $B_{2g}^{\rm ext}$ discussed in the text.

the interorbital pairing operators B_{2g} and $B_{2g}^{\rm ext}$ favored by numerical studies in a two-orbital model, present nodeless gaps on the hole pockets but nodes appear on the electron pockets.

V. CONCLUSIONS

In this work, a simple three-orbital Hamiltonian has been constructed involving the $3d$ orbitals xz, yz, and xy. These orbitals have the largest weight at the FS of the pnictide LaOFeAs, according to LDA calculations. It was shown that it is possible to qualitatively reproduce the shape of the LDA-FS by fixing the electron filling to 4 electrons per Fe. Moreover, two features that have been criticized in the two-orbital model have now been corrected: both hole pockets now arise from bands degenerate at the Γ-point, and there is no pocket around M in the extended BZ. In addition, the xy character of a small piece of the electron pockets is now properly reproduced.

Numerical calculations using a small 2×2 lattice show a tendency to the development of magnetic $(\pi,0)$-$(0,\pi)$ stripes when Coulombic interactions are added, result consistent with experimental observations. A mean-field analysis confirms this tendency for physically relevant values of J/U. As in the case of the two-orbital model, an antiferromagnetic metallic phase occurs only at intermediate values of the Coulomb repulsion. At large U, the ground state is magnetic, but it is an insulator that is also orbitally ordered. Additionally, a metallic, magnetic and orbitally ordered phase is encountered just before the metal-insulator transition. In the most interesting regime with a spin-$(\pi,0)$ antiferromagnetic metal without pronounced orbital order, the bands are similar to the uncorrelated ones, but their bandwidth is reduced with increasing U. The Fermi surface is also very similar to the uncorrelated one but, depending on U, we find small additional electron-like pockets near the original hole pockets around Γ (small U) or hole-like pockets between the electron- and hole-pockets (at slightly larger U).

The possible pairing operators that are allowed by the symmetry of the lattice and the orbitals have been constructed for pairs made of electrons separated by a distance up to one diagonal lattice spacing. If on-site pairing is disregarded due to the large Coulomb repulsion, it was found that the only purely intraband pairing operator that has a full gap on the FS is #I with $f(\mathbf{k}) = \cos k_x \cos k_y$ which corresponds to the $s\pm$ pairing operator with a momentum dependent OP that has opposite signs on the hole and electron FSs. This operator arises from a purely intraband pairing attraction equal for each of the three bands. Note that the pairing operator #I is the *only* one that leads to purely intraband pairing interactions. Since this pairing operator is proportional to the identity matrix λ_0 both in the orbital and the band representations we found that the ratio $|\Delta_i/\Delta_j|$ between the gaps in two different FSs can differ only by the ratios $|f(\mathbf{k}_i)/f(\mathbf{k}_j)|$; then, any experimental indication of a different kind of ratio would indicate some degree of interband pairing.[69] Thus, order parameter ratios predicted by several authors[50,73–75] with calculations based on purely intraband pairing (they allow interband hopping of intraband pairs) are not allowed by the symmetry of the lattice and the orbitals. In this regard, our calculations seem to indicate that unrelated gaps in different FSs can occur only in systems in which at least one orbital (or a group of orbitals) is not strongly hybridized with the remaining ones.

We found that all the other pairing operators, except for #I, lead to interband pairing attraction in the band representation. In addition, all the pairing operators with interband pairing studied here have nodal band structures at small V with the exception of pairing operator s_{IB}. In this case, the gap on the electron pockets is expected to have a stronger variation at different points in the BZ that the gap at the hole pockets. Thus, a strong indication that $s\pm$ is the appropriate pairing symmetry would be provided by experiments in the pnictides showing a nodeless gap in all FSs, relatively independent of momentum, and with similar values on all FSs.

Summarizing, we have shown that the addition of a third orbital corrects the shortcomings pointed out in

the two-orbital model: the two hole pockets now arise from bands degenerate at the Γ point while the electron pockets contain a small piece with xy character. However, the dependence of the magnetic phases with U for the undoped case appears to be similar for three and two orbitals except for a magnetic, orbital ordered, metallic phase that appears in the three-orbital case. In both models it is found that the only pairing operator allowed by symmetry with next or diagonal nearest-neighbor interactions which is purely intraband and produces a nodeless gap is the $s\pm$ state. In addition, the only change observed in the interorbital B_{2g} pairing state, favored by numerical simulations in the two-orbital model, is that, at the mean-field level, the addition of the xy orbital renders the gap on the hole pockets nodeless for much smaller values of the pairing attraction.

VI. ACKNOWLEDGMENTS

This research was sponsored by the National Science Foundation grant DMR-0706020 (M.D., A.N., A.M., and E.D.) and the Division of Materials Science and Engineering, Office of Basic Energy Sciences, U.S. Department of Energy (A.M. and E.D.).

Appendix A: Mean-Field Equations

In this appendix, we discuss the mean-field approach used here to study the Hamiltonian given by the kinetic energy Eq. (4) and the onsite Coulomb interaction Eq. (11). Depending on the ordering vectors $\mathbf{q}_1$ and $\mathbf{q}_2$, listed in Table II, for magnetic and orbital order, the real-space unit cell contains one, two or four sites: One for the ferro-orbital and ferromagnetic case, four if both ordering vectors are different from each other and from $(0,0)$, and two in all other cases. Following Refs. 25,59, we only keep the expectation values of density operators, as given in Eqs. (12) and (13) in the Coulomb interaction Eq. (11). Together with Eq. (4), this determines the mean-field Hamiltonian, see below. We then solve the self-consistency equations for the six parameters n_{xy}, m_{xy}, n, m, p, and q in Eqs. (12) and (13) for various combinations of ordering momenta, see Tab. II, which corresponds to minimizing the total energy. This is done for all considered phases and the one with the lowest energy is taken to be the stable solution. Depending on the size of the unit cell, one to four momenta are coupled by the Coulomb interaction. In the following, we will provide the Hamiltonians for several ordering patterns with different unit cells. In all cases, the sums run over the whole extended BZ corresponding to the one-iron unit cell. The calculations were carried out in momentum space for up to 400×400 $\mathbf{k}$-points. We did not observe any pronounced dependence on the number of momenta, except for very small lattice sizes.

1. Ferromagnetic and Ferro-Orbital Order: One-Site Unit Cell

In this case $\mathbf{q}_1 = \mathbf{q}_2 = (0,0)$ and

$$\begin{aligned} H_{\rm MF}(\mathbf{k}) = H_{\rm TB}(\mathbf{k}) &+ U \sum_{\mathbf{k},\mu,\sigma} n_\mu d^\dagger_{\mathbf{k},\mu,\sigma} d_{\mathbf{k},\mu,\sigma} \\ &+ (2U' - J) \sum_{\mathbf{k},\mu\neq\nu,\sigma} n_\nu d^\dagger_{\mathbf{k},\mu,\sigma} d_{\mathbf{k},\mu,\sigma} \\ &- U \sum_{\mathbf{k},\mu,\sigma} \frac{\sigma}{2} m_\mu d^\dagger_{\mathbf{k},\mu,\sigma} d_{\mathbf{k},\mu,\sigma} \\ &- J \sum_{\mathbf{k},\mu\neq\nu,\sigma} \frac{\sigma}{2} m_\nu d^\dagger_{\mathbf{k},\mu,\sigma} d_{\mathbf{k},\mu,\sigma} + NC \ , \end{aligned} \tag{A1}$$

where $n_\mu = n_{xy}$, $m_\mu = m_{xy}$ for the xy orbital, and $n_\mu = n \pm p/2$, $m_\mu = m \pm q$ for xz and yz. The sum over $\mathbf{k}$ runs through the whole BZ, N is the number of lattice sites, and the constant C is given by

$$\begin{aligned} C = &-U \sum_\mu n_\mu^2 + U/4 \sum_\mu m_\mu^2 \\ &- (2U' - J) \sum_{\mu\neq\nu} n_\mu n_\nu + J/4 \sum_{\mu\neq\nu} m_\mu m_\nu \ . \end{aligned} \tag{A2}$$

2. Antiferromagnetic and Ferro-Orbital: Two-Site Unit Cell

For AF order with $\mathbf{q}_1 = (\pi,\pi)$, $(0,\pi)$ or $(\pi,0)$, the real-space unit cell doubles, and momenta $\mathbf{k}$ and $\mathbf{k}+\mathbf{q_1}$ are coupled by the interaction.

$$\begin{aligned} H_{\rm MF}(\mathbf{k}) = H_{\rm TB}(\mathbf{k}) &+ U \sum_{\mathbf{k},\mu,\sigma} n_\mu d^\dagger_{\mathbf{k},\mu,\sigma} d_{\mathbf{k},\mu,\sigma} \\ &+ (2U' - J) \sum_{\mathbf{k},\mu\neq\nu,\sigma} n_\nu d^\dagger_{\mathbf{k},\mu,\sigma} d_{\mathbf{k},\mu,\sigma} \\ &- U \sum_{\mathbf{k},\mu,\sigma} \frac{\sigma}{2} m_\mu d^\dagger_{\mathbf{k}+\mathbf{q}_1,\mu,\sigma} d_{\mathbf{k},\mu,\sigma} \\ &- J \sum_{\mathbf{k},\mu\neq\nu,\sigma} \frac{\sigma}{2} m_\nu d^\dagger_{\mathbf{k}+\mathbf{q}_1,\mu,\sigma} d_{\mathbf{k},\mu,\sigma} + NC \ . \end{aligned} \tag{A3}$$

Again, $n_\mu = n_{xy}$, $m_\mu = m_{xy}$ for the xy orbital, and $n_\mu = n \pm p/2$, $m_\mu = m \pm q$ for xz and yz; and the same constant Eq. (A2) as above. The case of ferromagnetic order and alternating orbitals is treated in an analogous manner.

3. Antiferromagnetic and Alternating Orbital Order with the Same Ordering Vector: Two-Site Unit Cell

In some phases, both the orbital and the magnetic order alternate with the same ordering vector $\mathbf{q} = \mathbf{q}_1 =$

$\mathbf{q}_2 = (\pi,\pi)$, $(0,\pi)$ or $(\pi,0)$. In this case, the Hamiltonian is given by

$$\begin{aligned} H_{\rm MF}(\mathbf{k}) &= H_{\rm TB}(\mathbf{k}) \\ &+ [(4U'-2J)n + Un_{xy}] \sum_{\mathbf{k},\sigma} d^\dagger_{\mathbf{k},xy,\sigma} d_{\mathbf{k},xy,\sigma} \\ &+ [Un + (2U'-J)(n_{xy}+n)] \sum_{\substack{\mathbf{k},\sigma \\ \mu=xz,yz}} d^\dagger_{\mathbf{k},\mu,\sigma} d_{\mathbf{k},\mu,\sigma} \\ &- (U+J)q \sum_{\substack{\mathbf{k},\sigma \\ \mu=xz,yz}} \frac{\sigma\alpha}{2} d^\dagger_{\mathbf{k},\mu,\sigma} d_{\mathbf{k},\mu,\sigma} \\ &- [(U+J)m + Jm_{xy}] \sum_{\substack{\mathbf{k},\sigma \\ \mu=xz,yz}} \frac{\sigma}{2} d^\dagger_{\mathbf{k}+\mathbf{q}_1,\mu,\sigma} d_{\mathbf{k},\mu,\sigma} \\ &- (Um_{xy} + 2Jm) \sum_{\mathbf{k},\sigma} \frac{\sigma}{2} d^\dagger_{\mathbf{k}+\mathbf{q}_1,xy,\sigma} d_{\mathbf{k},xy,\sigma} \\ &+ (U-2U'-J)p \sum_{\substack{\mathbf{k},\sigma \\ \mu=xz,yz}} \frac{\alpha}{2} d^\dagger_{\mathbf{k}+\mathbf{q}_1,\mu,\sigma} d_{\mathbf{k},\mu,\sigma} + NC. \end{aligned} \tag{A4}$$

Here, $\alpha = \pm 1$ distinguishes between the xz and yz orbital flavors as σ does for the spin. The constant C reads

$$\begin{aligned} C = &-U(n_{xy}^2 - m_{xy}^2/4) - U(n^2 + p^2/2 - m^2/2 - q^2/2) \\ &- (8U'-4J)n_{xy}n - (4U'-2J)(n^2 - p^2/4) \\ &+ Jm_{xy}m + J(m^2 - q^2)/2\,. \end{aligned} \tag{A5}$$

4. Antiferromagnetic and Alternating Orbitals with Different Ordering Momenta: Four-Site Unit Cell

If both orbital occupation and magnetic order alternate with different ordering momenta, so that $\mathbf{q}_i = (\pi,\pi)$, $(0,\pi)$ or $(\pi,0)$ with $\mathbf{q}_1 \neq \mathbf{q}_2$, the real-space unit cell contains four sites, and consequently all four momenta $\mathbf{k}$, $\mathbf{k}+\mathbf{q}_1$, $\mathbf{k}+\mathbf{q}_2$, $\mathbf{k}+\mathbf{q}_1+\mathbf{q}_2$ are coupled, but apart from this, the Hamiltonian is very similar to the previous case:

$$\begin{aligned} H_{\rm MF}(\mathbf{k}) &= H_{\rm TB}(\mathbf{k}) \\ &+ [(4U'-2J)n + Un_{xy}] \sum_{\mathbf{k},\sigma} d^\dagger_{\mathbf{k},xy,\sigma} d_{\mathbf{k},xy,\sigma} \\ &+ [Un + (2U'-J)(n_{xy}+n)] \sum_{\substack{\mathbf{k},\sigma \\ \mu=xz,yz}} d^\dagger_{\mathbf{k},\mu,\sigma} d_{\mathbf{k},\mu,\sigma} \\ &- [(U+J)m + Jm_{xy}] \sum_{\substack{\mathbf{k},\sigma \\ \mu=xz,yz}} \frac{\sigma}{2} d^\dagger_{\mathbf{k}+\mathbf{q}_1,\mu,\sigma} d_{\mathbf{k},\mu,\sigma} \\ &- (Um_{xy} + 2Jm) \sum_{\mathbf{k},\sigma} \frac{\sigma}{2} d^\dagger_{\mathbf{k}+\mathbf{q}_1,xy,\sigma} d_{\mathbf{k},xy,\sigma} \\ &+ (U-2U'-J)p \sum_{\substack{\mathbf{k},\sigma \\ \mu=xz,yz}} \frac{\alpha}{2} d^\dagger_{\mathbf{k}+\mathbf{q}_2,\mu,\sigma} d_{\mathbf{k},\mu,\sigma} \\ &- (U-J)q \sum_{\substack{\mathbf{k},\sigma \\ \mu=xz,yz}} \frac{\sigma\alpha}{2} d^\dagger_{\mathbf{k}+\mathbf{q}_1+\mathbf{q}_2,\mu,\sigma} d_{\mathbf{k},\mu,\sigma} + NC. \end{aligned} \tag{A6}$$

The constant C is still given by equation (A5).

Appendix B: λ_i matrices

The λ_i matrices used in the text are presented here:

$$\lambda_0 = \begin{pmatrix} 1 & 0 & 0 \\ 0 & 1 & 0 \\ 0 & 0 & 1 \end{pmatrix}, \quad \lambda_1 = \begin{pmatrix} 0 & 1 & 0 \\ 1 & 0 & 0 \\ 0 & 0 & 0 \end{pmatrix},$$

$$\lambda_2 = \begin{pmatrix} 0 & -i & 0 \\ i & 0 & 0 \\ 0 & 0 & 0 \end{pmatrix}, \quad \lambda_3 = \begin{pmatrix} 1 & 0 & 0 \\ 0 & -1 & 0 \\ 0 & 0 & 0 \end{pmatrix},$$

$$\lambda_4 = \begin{pmatrix} 0 & 0 & 1 \\ 0 & 0 & 0 \\ 1 & 0 & 0 \end{pmatrix}, \quad \lambda_5 = \begin{pmatrix} 0 & 0 & -i \\ 0 & 0 & 0 \\ i & 0 & 0 \end{pmatrix},$$

$$\lambda_6 = \begin{pmatrix} 0 & 0 & 0 \\ 0 & 0 & 1 \\ 0 & 1 & 0 \end{pmatrix}, \quad \lambda_7 = \begin{pmatrix} 0 & 0 & 0 \\ 0 & 0 & -i \\ 0 & i & 0 \end{pmatrix},$$

$$\lambda_8 = \frac{1}{\sqrt{3}} \begin{pmatrix} 1 & 0 & 0 \\ 0 & 1 & 0 \\ 0 & 0 & -2 \end{pmatrix}.$$

* Electronic address: M.Daghofer@ifw-dresden.de; Present address: IFW Dresden, P.O. Box 27 01 16, D-01171 Dresden, Germany

1. Y. Kamihara, T. Watanabe, M. Hirano, and H. Hosono, J. Am. Chem. Soc **130**, 3296 (2008).
2. G. F. Chen, Z. Li, G. Li, J. Zhou, D. Wu, J. Dong, W. Z. Hu, P. Zheng, Z. J. Chen, H. Q. Yuan, J. Singleton, J. L. Luo, and N. L. Wang, Phys. Rev. Lett. **101**, 057007 (2008).
3. G. F. Chen, Z. Li, D. Wu, G. Li, W. Z. Hu, J. Dong, P. Zheng, J. L. Luo, and N. L. Wang, Phys. Rev. Lett. **100**, 247002 (2008).
4. H.-H. Wen, G. Mu, L. Fang, H. Yang, and X. Zhu, EPL **82**, 17009 (2008).
5. X. H. Chen, T. Wu, G. Wu, R. H. Liu, H. Chen, and D. F. Fang, Nature **453**, 761 (2008).
6. Z. Ren, J. Yang, W. Lu, W. Yi, G. Che, X. Dong, L. Sun, and Z. Zhao, Mater. Res. Innovat. **12**, 105 (2008).
7. Z.-A. Ren, W. Lu, J. Yang, W. Yi, X.-L. Shen, Z.-C. Li, G.-C. Che, X.-L. Dong, L.-L. Sun, F. Zhou, and Z.-X. Zhao, Chin. Phys. Lett. **25**, 2215 (2008).

[8] Z.-A. Ren, G.-C. Che, X.-L. Dong, J. Yang, W. Lu, W. Yi, X.-L. Shen, Z.-C. Li, L.-L. Sun, F. Zhou, and Z.-X. Zhao, EPL **83**, 17002 (2008).

[9] L. Boeri, O. V. Dolgov, and A. A. Golubov, Phys. Rev. Lett. **101**, 026403 (2008).

[10] J. Dong, H. J. Zhang, G. Xu, Z. Li, G. Li, W. Z. Hu, D. Wu, G. F. Chen, X. Dai, J. L. Luo, Z. Fang, and N. L. Wang, EPL **83**, 27006 (2008).

[11] C. de la Cruz, Q. Huang, J. W. Lynn, J. Li, W. Ratcliff II, J. L. Zarestky, H. A. Mook, G. F. Chen, J. L. Luo, N. L. Wang, and P. Dai, Nature **453**, 899 (2008).

[12] Y. Chen, J. W. Lynn, J. Li, G. Li, G. F. Chen, J. L. Luo, N. L. Wang, P. Dai, C. de la Cruz, and H. A. Mook, Phys. Rev. B **78**, 064515 (2008).

[13] C. Krellner, N. Caroca-Canales, A. Jesche, H. Rosner, A. Ormeci, and C. Geibel, Phys. Rev. B **78**, 100504(R) (2008).

[14] A. I. Goldman, D. N. Argyriou, B. Ouladdiaf, T. Chatterji, A. Kreyssig, S. Nandi, N. Ni, S. L. Bud'ko, P. C. Canfield, and R. J. McQueeney, Phys. Rev. B **78**, 100506(R) (2008).

[15] E. Dagotto, Rev. Mod. Phys. **66**, 763 (1994).

[16] S. Lebegue, Phys. Rev. B **75**, 035110 (2007).

[17] D. J. Singh and M.-H. Du, Phys. Rev. Lett. **100**, 237003 (2008).

[18] G. Xu, W. Ming, Y. Yao, X. Dai, S.-C. Zhang, and Z. Fang, EPL **82**, 67002 (2008).

[19] C. Cao, P. J. Hirschfeld, and H.-P. Cheng, Phys. Rev. B **77**, 220506(R) (2008).

[20] H.-J. Zhang, G. Xu, X. Dai, and Z. Fang, Chin. Phys. Lett. **26**, 017401 (2009).

[21] Y. Zhang, B. Zhou, F. Chen, J. Wei, M. Xu, L. X. Yang, C. Fang, W. F. Tsai, G. H. Cao, Z. A. Xu, M. Arita, C. Hong, K. Shimada, H. Namatame, M. Taniguchi, J. P. Hu, and D. L. Feng, arXiv:0904.4022v1 (unpublished)

[22] S. Raghu, X.-L. Qi, C.-X. Liu, D. J. Scalapino, and S.-C. Zhang, Phys. Rev. B **77**, 220503(R) (2008).

[23] M. Daghofer, A. Moreo, J. A. Riera, E. Arrigoni, D. J. Scalapino, and E. Dagotto, Phys. Rev. Lett. **101**, 237004 (2008).

[24] A. Moreo, M. Daghofer, J. A. Riera, and E. Dagotto, Phys. Rev. B **79**, 134502 (2009).

[25] R. Yu, K. T. Trinh, A. Moreo, M. Daghofer, J. A. Riera, S. Haas, and E. Dagotto, Phys. Rev. B **79**, 104510 (2009).

[26] F. Lu and L.-J. Zou, J. Phys.: Condens. Matter **21**, 255701 (2009).

[27] W.-Q. Chen, K.-Y. Yang, Y. Zhou, and F.-C. Zhang, Phys. Rev. Lett. **102**, 047006 (2009).

[28] M. J. Calderon, B. Valenzuela, and E. Bascones, New J. Phys. **11**, 013051 (2009).

[29] K. Kubo and P. Thalmeier, J. Phys. Soc. Jpn. **78** (2009).

[30] C.-C. Lee, W.-G. Yin, and W. Ku, Phys. Rev. Lett. **103**, 267001 (2009).

[31] P. A. Lee and X.-G. Wen, Phys. Rev. B **78**, 144517 (2008).

[32] E. Dagotto, T. Hotta, and A. Moreo, Phys. Rep. **344**, 1 (2001).

[33] L. Shan, Y. Wang, X. Zhu, G. Mu, L. Fang, C. Ren, and H.-H. Wen, EPL **83**, 57004 (2008).

[34] M. Gang, Z. Xi-Yu, F. Lei, S. Lei, R. Cong, and W. Hai-Hu, Chin. Phys. Lett. **25**, 2221 (2008).

[35] C. Ren, Z.-S. Wang, H. Yang, X. Zhu, L. Fang, G. Mu, L. Shan, and H.-H. Wen, arXiv:0804.1726 (unpublished)

[36] K. Ahilan, F. L. Ning, T. Imai, A. S. Sefat, R. Jin, M. A. McGuire, B. C. Sales, and D. Mandrus, Phys. Rev. B **78**, 100501(R) (2008).

[37] Y. Nakai, K. Ishida, Y. Kamihara, M. Hirano, and H. Hosono, J. Phys. Soc. Jpn. **77**, 073701 (2008).

[38] H.-J. Grafe, D. Paar, G. Lang, N. J. Curro, G. Behr, J. Werner, J. Hamann-Borrero, C. Hess, N. Leps, R. Klingeler, and B. Büchner, Phys. Rev. Lett. **101**, 047003 (2008).

[39] Y.-L. Wang, L. Shan, L. Fang, P. Cheng, C. Ren, and H.-H. Wen, Supercond. Sci. Technol. **22**, 015018 (2009).

[40] K. Matano, Z. A. Ren, X. L. Dong, L. L. Sun, Z. X. Zhao and G. Zheng, EPL **83**, 57001 (2008).

[41] H. Mukuda, N. Terasaki, H. Kinouchi, M. Yashima, Y. Kitaoka, S. Suzuki, S. Miyasaka, S. Tajima, K. Miyazawa, P. Shirage, H. Kito, H. Eisaki, and A. Iyo, J. Phys. Soc. Jpn. **77**, 093704 (2008).

[42] O. Millo, I. Asulin, O. Yuli, I. Felner, Z.-A. Ren, X.-L. Shen, G.-C. Che, and Z.-X. Zhao, Phys. Rev. B **78**, 092505 (2008).

[43] X. L. Wang, S. X. Dou, Z.-A. Ren, W. Yi, Z.-C. Li, Z.-X. Zhao, and S.-I. Lee, J. Phys.: Condens. Matter **21**, 205701 (2009).

[44] K. Hashimoto, T. Shibauchi, T. Kato, K. Ikada, R. Okazaki, H. Shishido, M. Ishikado, H. Kito, A. Iyo, H. Eisaki, S. Shamoto, and Y. Matsuda, Phys. Rev. Lett. **102**, 017002 (2009).

[45] T. Kondo, A. F. Santander-Syro, O. Copie, C. Liu, M. E. Tillman, E. D. Mun, J. Schmalian, S. L. Bud'ko, M. A. Tanatar, P. C. Canfield, and A. Kaminski, Phys. Rev. Lett. **101**, 147003 (2008).

[46] H. Ding, P. Richard, K. Nakayama, K. Sugawara, T. Arakane, Y. Sekiba, A. Takayama, S. Souma, T. Sato, T. Takahashi, Z. Wang, X. Dai, Z. Fang, G. F. Chen, J. L. Luo, and N. L. Wang, EPL **83**, 47001 (2008).

[47] K. Nakayama, T. Sato, P. Richard, Y.-M. Xu, Y. Sekiba, S. Souma, G. F. Chen, J. L. Luo, N. L. Wang, H. Ding, T. Takahashi, EPL **85**, 67002 (2009).

[48] C. Martin, M. E. Tillman, H. Kim, M. A. Tanatar, S. K. Kim, A. Kreyssig, R. T. Gordon, M. D. Vannette, S. Nandi, V. G. Kogan, S. L. Bud'ko, P. C. Canfield, A. I. Goldman, and R. Prozorov, Phys. Rev. Lett. **102**, 247002 (2009).

[49] T. Y. Chen, Z. Tesanovic, R. H. Liu, X. H. Chen, and C. L. Chien, Nature **453**, 1224 (2008).

[50] D. Parker, O. V. Dolgov, M. M. Korshunov, A. A. Golubov, and I. I. Mazin, Phys. Rev. B **78**, 134524 (2008).

[51] G. Mu, H. Luo, Z. Wang, L. Shan, C. Ren, and H.-H. Wen, Phys. Rev. B **79**, 174501 (2009).

[52] S.-L. Yu, J. Kang, and J.-X. Li, Phys. Rev. B **79**, 064517 (2009).

[53] F. Krüger, S. Kumar, J. Zaanen, and J. van den Brink, Phys. Rev. B **79**, 054504 (2009).

[54] K. Haule, J. H. Shim, and G. Kotliar, Phys. Rev. Lett. **100**, 226402 (2008).

[55] I. I. Mazin, D. J. Singh, M. D. Johannes, and M. H. Du, Phys. Rev. Lett. **101**, 057003 (2008).

[56] K. Kuroki, S. Onari, R. Arita, H. Usui, Y. Tanaka, H. Kontani, and H. Aoki, Phys. Rev. Lett. **101**, 087004 (2008).

[57] Choosing $t_8 = +t_7/2$ would also give us the desired results: The purely xy character is then found along the X-M and Y-M directions, which are equivalent to Γ-X and Γ-Y in the reduced BZ.

[58] Another way to obtain yz character between the X and M points of the extended BZ would be to choose t_3 and t_4 very large and t_6 much smaller, so that the xy band would remain below the Fermi surface and xz/yz rise above it. However, the degeneracy of xz and yz at $M = (\pi, \pi)$ would

then force an additional hole pocket around M similar to the FS in Ref. 31.
[59] T. Nomura and K. Yamada, J. Phys. Soc. Jpn. **69**, 1856 (2000).
[60] Note that the large number of inter- as well as intra-orbital hopping processes between NN and NNN sites renders the usual Goodenough-Kanamori rules inapplicable.
[61] W. L. Yang, A. P. Sorini, C-C. Chen, B. Moritz, W.-S. Lee, F. Vernay, P. Olalde-Velasco, J. D. Denlinger, B. Delley, J.-H. Chu, J. G. Analytis, I. R. Fisher, Z. A. Ren, J. Yang, W. Lu, Z. X. Zhao, J. van den Brink, Z. Hussain, Z.-X. Shen, and T. P. Devereaux, Phys. Rev. B **80**, 014508 (2009)
[62] S. Haas, A. Moreo, and E. Dagotto, Phys. Rev. Lett. **74**, 4281 (1995); and references therein.
[63] M. Yi, D.H. Lu, J.G. Analytis, J.-H. Chu, S.-K. Mo, R.-H. He, M. Hashimoto, R.G. Moore, I.I. Mazin, D.J. Singh, Z. Hussain, I.R. Fisher, and Z.-X. Shen, Phys. Rev. B **80**, 174510 (2009)
[64] Z.-H. Wang, H. Tang, Z. Fang, and X. Dai, arXiv:0805.0736 (unpublished)
[65] J. Shi, arXiv:0806.0259 (unpublished)
[66] W.-L. You, S.-J. Gu, G.-S. Tian, and H.-Q. Lin, Phys. Rev. B **79**, 014508 (2009).
[67] Y. Wan and Q.-H. Wang, EPL **85**, 57007 (2009).
[68] L. Schiff, *Quantum Mechanics*, 3 ed. (McGraw-Hill Kogakusha, Tokyo, 1968).
[69] A. Moreo, M. Daghofer, A. Nicholson, and E. Dagotto, Phys. Rev. B **80**, 104507 (2009).
[70] J. Nagamatsu, N. Nakagawa, T. Muranaka, Y. Zenitani, and J. Akimitsu, Nature **410**, 63 (2001).
[71] H. J. Choi, D. Roundy, H. Sun, M. L. Cohen, and S. G. Louie, Nature **418**, 758 (2002).
[72] Note that the "interband" superconductivity proposed by some authors[50,73–75] is still represented by an intraband (i.e., diagonal) pairing matrix but with $\Delta_1 = \Delta_1(\Delta_2, \Delta_3)$, $\Delta_2 = \Delta_2(\Delta_1, \Delta_3)$, and $\Delta_3 = \Delta_3(\Delta_1, \Delta_2)$.
[73] Y. Bang and H.-Y. Choi, Phys. Rev. B **78**, 134523 (2008).
[74] K. Seo, A.B. Bernevig and J.P. Hu, Phys. Rev. Lett. **101**, 206404 (2008); M.M. Parish, J.P. Hu, and B.A. Bernevig, Phys. Rev. B **78**, 144514 (2008).
[75] O.V. Dolgov, I.I. Mazin, D. Parker, and A.A. Golubov, Phys. Rev. B **79**, 060502(R) (2009).